Electron energy-loss spectra of coupled electronic states: Effects of Rydberg-valence interactions in O_2

B. R. Lewis, J. P. England, and S. T. Gibson
Research School of Physical Sciences and Engineering, The Australian National University, Canberra ACT 0200, Australia

M. J. Brunger
School of Chemistry, Physics and Earth Sciences, The Flinders University of South Australia, Bedford Park SA 5042, Australia

M. Allan
Institut de Chimie Physique, Université de Fribourg, Pérolles, CH-1700 Fribourg, Switzerland
(Received 17 July 2000; published 11 January 2001)

The concept of the ''generalized transition moment'' is extended beyond the region of applicability of the first Born approximation and is used in the analysis of electron energy-loss spectra for O_2, presented here, which have been measured at intermediate impact energies. A coupled-channel theoretical treatment of the strongly mixed Rydberg and valence states that dominate the optically allowed spectrum is used to explain the relative intensities of many unusual features occurring in the 7–11.2-eV energy-loss region. For these electronically excited states of $^3\Sigma_u^-$ and $^3\Pi_u$ symmetry, the evolution of the shape of the corresponding electron energy-loss spectrum as the scattering conditions are changed is controlled essentially by one parameter: the ratio of the diabatic generalized transition moments into the Rydberg and valence components of the mixed electronic states. The generalized Rydberg transition moment is found to decrease much faster than the valence moment as the momentum transferred in the collision increases. The results of the coupled-channel analysis also indicate that the more diffuse spectral features are generally asymmetric, those in the 7–9.8-eV region changing slightly in position as the scattering conditions are altered. Thus, the Gaussian–line-shape-based models that have been employed previously in attempts to decompose the diffuse part of the electron energy-loss spectrum for O_2, into contributions from different electronic states, are unlikely to have given meaningful results. As a consequence of the Rydberg-valence interactions, it is found that some vibrational levels of the mixed states give rise to features in the electron energy-loss spectrum which are anomalously strong at the low impact energies and large scattering angles for which normal optically allowed transitions are expected to decline in relative strength. These ''persistent lines'' are easily confused with those from the optically forbidden transitions which increase in relative intensity under such conditions. Thus, the coupled-channel technique is found to be a valuable aid to the assignment of features in the electron energy-loss spectrum.

DOI: 10.1103/PhysRevA.63.022707 PACS number(s): 34.80.Gs, 34.50.Gb

I. INTRODUCTION

Electron energy-loss (EEL) spectra of molecules, despite an energy resolution which is limited when compared with corresponding optical spectra, provide valuable information on the molecular structure of excited states which may be unobtainable by other means. In particular, the relaxation of the optical selection rules for electronic transitions in EEL spectra, taken under conditions of significant momentum transfer, results in the observation of features which are not seen in the optical spectrum. For example, the $3s\sigma_g\, C\,^3\Pi_g$ and $3s\sigma_g\, d\,^1\Pi_g$ Rydberg states of O_2, the molecule of principal interest to this work, were identified first from peaks in EEL spectra [1,2].

As an aid to the deconvolution and assignment of features in EEL spectra, it is often assumed that the relative vibrational intensities for a given electronic transition are independent of the incident-electron energy and scattering angle and are proportional to the optical Franck-Condon factors [3–9]. Indeed, this assumption has been verified experimentally for a number of well behaved molecular transitions, e.g., the fourth-positive system of CO, $A\,^1\Pi \leftarrow X\,^1\Sigma^+$, in detailed work by Lassettre and co-workers [7,10–13]. As has been noted by Lassettre [12], these experimental studies have been conducted for a wide range of kinematical conditions, including incident energies for which the first Born approximation (FBA) cannot be expected to hold. However, anomalous behavior of the relative vibrational intensities has been observed for some transitions, notably the $B\,^1\Sigma^+ \leftarrow X\,^1\Sigma^+$ transition of CO [14] and the $E\,^3\Sigma_u^- \leftarrow X\,^3\Sigma_g^-$ [15] transition of O_2 [2,12,16,17]. In the case of the $E \leftarrow X$ transition, the relative intensities of the peaks in the EEL spectra at 9.97-, 10.28-, and 10.57-eV energy loss varied so dramatically with the kinematical conditions that it was not apparent originally that these features were vibrational bands associated with a single electronic transition.

In an important study which was, however, restricted to scattering conditions under which the FBA was valid, Dillon *et al.* [17] showed that anomalous behavior of the vibrational intensities is associated with upper states having a strongly mixed electronic character. In particular, interacting states whose adiabatic potential-energy curves exhibit a strongly avoided crossing, for example, Rydberg and valence states of the same symmetry, may be expected to show a non-Franck-Condon distribution of vibrational intensities. It is well

known [18–21] that some of the $3p\pi_u$ and $3p\sigma_u$ Rydberg states of O_2 interact strongly with valence states and this molecule is, therefore, expected to provide fertile ground for a study of anomalous relative intensities in EEL spectra in the ~7–12-eV energy-loss region.

The optical spectrum of O_2 in this range consists principally of electric-dipole-allowed transitions into the mixed Rydberg-valence states of $^3\Sigma_u^-$ and $^3\Pi_u$ symmetry. The dominant $^3\Sigma_u^- \leftarrow X\,^3\Sigma_g^-$ features comprise the well-known Schumann-Runge (SR) continuum, $B\,^3\Sigma_u^- \leftarrow X\,^3\Sigma_g^-$, and Tanaka's progression I [22], consisting of the *longest*, *second*, and *third* bands at excitation energies of 9.97, 10.28, and 10.57 eV, respectively. The SR-continuum cross section has been reviewed by Hudson [23], and, more recently, by Chan *et al.* [24]. There has been considerable argument, reviewed by Lewis *et al.* [25], over electronic and vibrational assignments for the longest, second, and third bands. Following *ab initio* calculations of Rydberg-valence mixing in the $^3\Sigma_u^-$ states of O_2 [18–20,26], and the arguments of Katayama *et al.* [27], it is clear that these bands are part of a single progression, as envisaged originally by Tanaka [22]. They are the (0,0)–(2,0) bands of the $E\,^3\Sigma_u^- \leftarrow X\,^3\Sigma_g^-$ transition. The *E* and *B* states undergo an avoided crossing in the energy region of interest to this study, explaining the anomalous behavior of the $E \leftarrow X$ system and previous difficulties in the assignment of the corresponding spectrum. Although the $^3\Pi_u$ states exhibit a similar avoided crossing [18], the resultant spectrum is less prominent than in the $^3\Sigma_u^-$ case since the electronic transition moment for the $^3\Pi_u \leftarrow X\,^3\Sigma_g^-$ *valence* transition is unusually small [28]. However, measurements of the quantum yield for the production of $O(^1D)$ in the photodissociation of O_2 [29–32] show features in the $O(^3P)+O(^3P)$ dissociation channel at 9.15-, 10.66-, and 10.76-eV excitation energies which are associated with $^3\Pi_u \leftarrow X\,^3\Sigma_g^-$ transitions. Theoretical treatments of the Rydberg-valence interactions for the $^3\Pi_u$ states [33–35] have shown that the $J\,^3\Pi_u$ and $F\,^3\Pi_u$ states [36] undergo an avoided crossing in the energy region of interest to this study, and that the 9.15-eV band is a diffuse resonance associated with a plateau in the $J\,^3\Pi_u$-state potential-energy curve, while the bands at 10.66 and 10.76 eV are the (0,0) and (1,0) bands of the $F\,^3\Pi_u \leftarrow X\,^3\Sigma_g^-$ transition.

All of the features in the optical spectrum of O_2 in the 7–12 eV range are, to a greater or lesser extent, diffuse due to predissociation or direct dissociation. The application [37] of the techniques of scattering theory [38,39] to describe the *half collisions* involved in molecular photodissociation has led to several coupled-channel (CC) studies that have analyzed quantitatively the O_2 Rydberg-valence interactions. Using the CC formalism of Torop *et al.* [40] to account for the interactions of the lowest $^3\Sigma_u^-$ states, Wang *et al.* [41] successfully explained the measured temperature coefficient of the O_2 photodissociation cross section in the 7.7–9.5-eV range, and, in related work [42], also succeeded in explaining quantitatively the anomalous isotopic shift, linewidth, and line-shape asymmetry observed for the longest band. More recently, England *et al.* [35], using a CC model that treated the interactions between the lowest valence state of $^3\Pi_u$ symmetry and the $^3\Pi_u$ Rydberg states with principal quantum numbers from 3 to 7, have successfully explained the anomalous energy structure of the $^3\Pi_u \leftarrow X\,^3\Sigma_g^-$ predissociating resonances observed in the 10.5–11.5-eV region.

There have been many measurements of EEL spectra for O_2 in the 7–11.2-eV energy-loss region, covering a range of incident energies from near threshold to 25 keV and a range of scattering angles from 0° to 156°, with instrumental resolutions from 10-meV full width at half maximum (FWHM) to 200-meV FWHM. These studies fall loosely into two groups. First, measurements of EEL spectra for high-impact energies and forward scattering have been performed [10,16,24,43–46], principally to enable the determination of generalized oscillator strengths for electronic excitation which could then be compared with the corresponding optical oscillator strengths by extrapolation to zero momentum transfer. These studies include the very-high-resolution (10-meV FWHM) spectra of Geiger and Schröder [16] and culminate in the dipole (e,e) spectra of Chan *et al.* [24], taken at keV impact energies under conditions of negligible momentum transfer, which are directly comparable with optical spectra. Second, low, and intermediate impact-energy EEL spectra have been measured for a range of scattering angles [1,2,4,47–49], principally to enable the determination of differential and integrated cross sections for electronic excitation, and to facilitate the discovery of electric-dipole-forbidden transitions of the oxygen molecule. The highest-resolution measurements in this group (20–25-meV FWHM) are those of Allan [4]. As noted in the reviews of Trajmar *et al.* [50], Trajmar and Cartwright [51], and Itikawa *et al.* [52], the measurements in this group are fragmentary, with large gaps in the kinematical conditions studied. Shyn *et al.* [53,54] have attempted to remedy this deficiency by analyzing a large number of spectra taken with impact energies from 15 to 50 eV and scattering angles from 12° to 156°, obtaining differential and integrated excitation cross sections for a number of decomposed spectral features. However, they published only one spectrum [53], making it difficult to assess the validity of their spectral decomposition. Spanning the two classes of spectra are the measurements of Wakiya [55], taken for impact energies from 20 to 500 eV and scattering angles from 5° to 130°. This is the only comprehensive data set available, but the spectra have not been decomposed into contributions from different electronic states.

Theoretical discussions of the relationship between optical and EEL spectra are normally conducted using the concept of the *generalized oscillator strength* (GOS), introduced by Bethe [56], and usually formulated within the FBA. In an important paper, however, Lassettre *et al.* [57] showed that, even if the FBA does not apply, a GOS can be defined which becomes the optical oscillator strength in the limit of vanishing momentum transfer. It follows from this that a *generalized transition moment* (GTM) can be defined which becomes the electric-dipole transition moment in the same limit.

In this work we are concerned with the evolution of the molecular EEL spectrum for electronic-vibrational excitation away from the optical spectrum, as the momentum transfer is increased. In particular, we address the characteristics of the

vibrational structure of the EEL spectra of coupled electronic states by extending the GTM concept beyond the region of applicabilty of the FBA, using a CC treatment of the radial wave functions for the target molecule which is known to describe the optical spectrum accurately. This treatment, which is a natural extension of the FBA theoretical approach of Dillon *et al.* [17], relies essentially on the adiabatic-nuclei (AN) approximation for electronic excitation [58] and results in the kinematical effects being contained in the GTMs for the interacting electronic states. The practical motivation for this work lies essentially in the desire to obtain an improved understanding of the factors determining the relative intensities of electronic-vibrational features in EEL spectra with a view to obtaining realistic spectral assignments. We illustrate the principles involved by performing a detailed CC analysis of some EEL spectra of the strongly mixed Rydberg-valence states of O_2 in the 7–11.2-eV energy-loss region. The spectra analyzed are the ''optical'' dipole (e,e) spectrum of Chan *et al.* [24], the low and intermediate impact-energy spectra of Allan [4], and some additional intermediate impact-energy spectra presented in this work. In addition, we analyze critically the spectral decomposition techniques used by Cartwright *et al.* [59] and Shyn *et al.* [53] to analyze the SR continuum.

II. EXPERIMENTAL METHOD

All spectra were recorded in the constant residual energy (CRE) mode, in which the energy loss W is varied by ramping the beam energy E_i and detecting electrons (scattered through an angle θ) having a fixed energy E_r. In the present study, we have supplemented previously reported EEL spectra for O_2 [4], measured at $E_r=20$ eV, $\theta=10°$, and $E_r=2$ eV, $\theta=90°$, with new measurements at $E_r=20$ eV, $\theta=0°$, 5°, 20°, 30° and $E_r=50$ eV, $\theta=0°$, 10°. In addition, angular-dependence spectra were measured for some spectral features in the energy-loss range $W=7$–11.2 eV for residual energies $E_r=20$ eV and 50 eV.

The experimental apparatus and the procedure for calibrating the instrumental response as a function of incident and residual energy have been described in detail elsewhere [60,61]. Briefly, an essentially standard electrostatic spectrometer, using hemispherical deflectors for electron energy selection and constructed with a careful choice of materials, was used under computer control to obtain an improved performance. The beam source and analyzer were differentially pumped by a 160-mm-diameter diffusion pump, the collision region by a 400-mm-diameter diffusion pump. This helped to ensure the long-term stability of the apparatus. O_2 (99.995%, less than 10 ppm N_2) was introduced into the collision region as an effusive beam through a nozzle kept at 317 ± 3 K. An energy resolution of $\sim$25-meV FWHM was achieved in the energy-loss spectra, together with an angular resolution varying from $\sim 1.5°$ FWHM at $E_r=50$ eV through $\sim 2.5°$ FWHM at $E_r=20$ eV, to $\sim 7°$ FWHM at $E_r=2$ eV. Due to the CRE mode of operation, it was not necessary to correct the EEL spectra for the instrumental response function in the particular energy-loss range $W=7$–11.2 eV of interest to us in this work. The angular-dependence spectra, measured by repetitively scanning the analyzer position with a stepping motor, were corrected using an average of the instrumental angular response functions applicable at the incident and residual energies [4].

III. THEORETICAL ASPECTS

In this work, we are concerned primarily with the *relative* intensities of electronic and vibrational features in the EEL spectra of molecules, particularly those associated with interacting Rydberg and valence states involved in optically allowed transitions. The following discussion is restricted to diatomic molecules and, unless stated otherwise, atomic units $(e=\hbar=m_e=1)$ are used throughout in the equations [62].

A. Kinematics

As implied in Sec. II, in EEL experiments, the current of electrons with an initial energy E_i and residual energy E_r, following scattering through an angle θ, is measured as a function of energy loss $W=E_i-E_r$, equal to the molecular excitation energy. The EEL cross section $\sigma(W,E_r,\theta)$ is directly related to the differential scattering cross section for electronic excitation. The momentum $\mathbf{K}$ transferred to the molecule in the scattering process is a fundamental quantity in the theory of electron scattering which may be obtained simply from kinematical considerations. If the initial and scattered electron momenta are given by $\mathbf{k}_i$ and $\mathbf{k}_r$, respectively, then, from conservation of momentum,

$$\mathbf{K}=\mathbf{k}_i-\mathbf{k}_r \tag{1}$$

and

$$K^2=k_i^2+k_r^2-2k_ik_r\cos\theta, \tag{2}$$

where K, k_i, and k_r are the magnitudes of $\mathbf{K}$, $\mathbf{k}_i$, and $\mathbf{k}_r$, respectively. From conservation of energy,

$$k_i^2-k_r^2=2W. \tag{3}$$

Equation (2) may be rewritten in terms of the experimental observables

$$K^2=4[E_r+W/2-\sqrt{E_r(W+E_r)}\cos\theta]. \tag{4}$$

B. Generalized transition parameters

The differential cross section for the electron-impact excitation of a molecule from a ground state Φ_0 to the electronic state Φ_n is given by the usual expression [63]

$$\left(\frac{d\sigma}{d\Omega}\right)=\frac{k_r}{k_i}|\mathcal{F}_{n0}(\mathbf{k}_r,\mathbf{k}_i)|^2, \tag{5}$$

where $\mathcal{F}_{n0}(\mathbf{k}_r,\mathbf{k}_i)$ is the scattering amplitude for electronic excitation. In the AN or nuclear-impulse approximation, where, classically, the collision time is significantly less than the periods for nuclear rotation and vibration, the molecular nuclei may be regarded as fixed during the collision. Under

these conditions, the Born-Oppenheimer (BO) approximation may be used to separate the nuclear and electronic variables in the wave function for the molecule-electron system [64]. In the frame-transformation picture of electron-molecule scattering [65,66], the AN approximation is tantamount to assuming that the fixed-nuclei (FN) approximation is applicable for all scattering electron-target distances, even in the long-range asymptotic region. This assumption is expected to be valid for nonresonant scattering with E_i well above threshold, provided that the scattering is not dominated by strong long-range interactions [63]. Under conditions for which the AN approximation is valid, the scattering amplitude for electronic-vibrational excitation may be expressed in the BO form as [58,63]

$$\mathcal{F}^{\mathrm{AN}}_{nv',0v''}(\mathbf{k}_r,\mathbf{k}_i)=\langle\chi_{nv'}(R)|\mathcal{F}^{\mathrm{FN}}_{n0}(\mathbf{k}_r,\mathbf{k}_i;R)|\chi_{0v''}(R)\rangle, \tag{6}$$

where $\mathcal{F}^{\mathrm{FN}}_{n0}(\mathbf{k}_r,\ \mathbf{k}_i;\ R)$ is the fixed-nuclei scattering amplitude for the electronic transition $n\leftarrow 0$, parametrically dependent on the internuclear separation R of the target diatom, and $\chi_{nv'}(R)$ and $\chi_{0v''}(R)$ are the unperturbed [67] radial wave functions for the final and initial states, respectively. Since rotational features are not observed generally in EEL spectra, we have suppressed the rotational quantum numbers in Eq. (6), labeling the radial wave functions by the upper- and lower-state vibrational quantum numbers, v' and v'', respectively. In their discussion of the AN approximation for the case of *electronic* excitation, Shugard and Hazi [58] noted that the range of applicability of Eq. (6) was restricted to impact energies well above threshold unless the potential-energy curves for the initial and final states were parallel in the Franck-Condon region. They [58] circumvented this difficulty, however, by suggesting that the formalism of Eq. (6) could be retained at impact energies closer to threshold by generalizing the FN scattering amplitude to an off-shell quantity, with a resultant explicit dependence on v'. In this case, it may be possible to subsume this v' dependence into an *effective* FN scattering amplitude in Eq. (6) with a different R dependence [68].

In this work, we are interested in comparisons between the optical and EEL spectra and it is, therefore, convenient to extend the notion of the generalized electronic oscillator strength (GEOS), defined by Bethe [56], and, by analogy, to introduce the adiabatic-nuclei generalized vibrational oscillator strength (AN-GVOS) defined by

$$f^{\mathrm{AN}}_{nv',0v''}(\mathbf{k}_r,\mathbf{k}_i)=\frac{K^2W}{2}|\mathcal{F}^{\mathrm{AN}}_{nv',0v'}(\mathbf{k}_r,\mathbf{k}_i)|^2. \tag{7}$$

Using Eq. (6), Eq. (7) may be rewritten as

$$f^{\mathrm{AN}}_{nv',0v''}(\mathbf{k}_r,\mathbf{k}_i)=2W|\langle\chi_{nv'}(R)|\mathcal{M}^{\mathrm{FN}}_{n0}(\mathbf{k}_r,\mathbf{k}_i;R)|\chi_{0v''}(R)\rangle|^2, \tag{8}$$

where

$$\mathcal{M}^{\mathrm{FN}}_{n0}(\mathbf{k}_r,\mathbf{k}_i;R)=-\frac{K}{2}\mathcal{F}^{\mathrm{FN}}_{n0}(\mathbf{k}_r,\mathbf{k}_i;R). \tag{9}$$

The corresponding fixed-nuclei generalized electronic oscillator strength (FN-GEOS) is given by

$$f^{\mathrm{FN}}_{n0}(\mathbf{k}_r,\mathbf{k}_i;R)=2W|\mathcal{M}^{\mathrm{FN}}_{n0}(\mathbf{k}_r,\mathbf{k}_i;R)|^2. \tag{10}$$

Equations (8) and (10) have forms similar to the equivalent expressions for the optical electronic and vibrational oscillator strengths f_{n0} and $f_{nv',0v''}$, respectively, with $\mathcal{M}^{\mathrm{FN}}_{n0}(\mathbf{k}_r,\ \mathbf{k}_i;\ R)$ playing the role of a *generalized electronic transition moment* (GETM).

In the first Born approximation, which is expected to apply over a more limited kinematical range than the AN approximation, following an explicit integration over the coordinates of the scattering electron, the corresponding scattering amplitude can be shown to be [17,69]

$$\mathcal{F}^{\mathrm{B}}_{n0}(\mathbf{K},R)=-\frac{2}{K^2}\left\langle\Phi_n\left|\sum_j\ \exp(i\mathbf{K}\cdot\mathbf{r}_j)\right|\Phi_0\right\rangle, \tag{11}$$

and the Born GETM is given by

$$\mathcal{M}^{B}_{n0}(\mathbf{K},R)=\left\langle\Phi_n\left|K^{-1}\sum_j\ \exp(i\mathbf{K}\cdot\mathbf{r}_j)\right|\Phi_0\right\rangle, \tag{12}$$

where Φ_n and Φ_0 are the electronic wave functions for the excited and ground states, respectively, and the summation is over the molecular electrons. As is well known [17,69], in the limit of vanishing momentum transfer $K\rightarrow 0$, the Born GETM is equal to the electric-dipole transition moment and the Born GEOS is equal to the optical oscillator strength. In addition, as noted in Sec. I, Lassettre *et al.* [57] showed that, *even if the Born approximation does not hold*, the GEOS still becomes the optical oscillator strength in the $K\rightarrow 0$ limit. Thus, the relationship between the generalized and optical transition parameters may be regarded as formally established.

C. Relative intensities

In the adiabatic-nuclei approximation, the relative intensities of the individual vibrational levels of the AN-GVOS [Eq. (8)] are determined essentially by the behavior of the FN-GEOS as a function of $\mathbf{k}_r$, $\mathbf{k}_i$, and R. In the first Born approximation, the FN-GEOS is dependent specifically on K^2 and R. In their study, within the framework of the FBA, Dillon *et al.* [17] considered the problem of relative vibrational intensities using accurate multireference single- and double-excitation configuration-interaction (MRD-CI) calculations of the FN-GEOS for the $A\leftarrow X$ and $B\leftarrow X$ transitions of CO and the $E\leftarrow X$ transition of O_2. They [17] pointed out that the shape of the vibrational envelope of the GVOS for a given electronic transition would be preserved for different scattering angles if the FN-GEOS for different R values (in the Franck-Condon region) exhibited similar dependences on K^2, and their MRD-CI calculations indicated that such behavior was indeed to be expected for the $A\leftarrow X$ transition of CO. This computational result is consistent with the experimental observation [12] of vibrational GVOS envelopes which do not vary significantly with kinematical conditions

for several ''normal'' molecular transitions, including the $A \leftarrow X$ system of CO, where the upper states of those transitions exhibit no significant interactions with other electronic states. Conversely, the MRD-CI calculations of Dillon *et al.* [17] show conclusively that the vibrational GVOS envelopes for transitions involving upper states which are of significantly mixed character, involving avoided crossings between two states of like symmetry, may vary rapidly with the scattering conditions. This provides an explanation for the apparently anomalous behavior of some vibrational peaks in EEL spectra, e.g., in the $B \leftarrow X$ transition of CO and the $E \leftarrow X$ transition of O_2.

The experimental results discussed by Lassettre and coworkers [12,57] show conclusively that the GVOS vibrational envelopes in EEL spectra for a number of molecular transitions do not vary significantly with the kinematical conditions, even for impact energies where the FBA is not expected to apply. Lassettre [12] explained these observations using simple arguments, based on the Franck-Condon principle, which were not dependent on the projectile energy, and Lassettre *et al.* [57] suggested that the concept and definition of the GEOS be extended into kinematical regions where the FBA is invalid. The adiabatic-nuclei approximation assumed in this work is consistent with these observations and suggestions. The AN-GVOS is given by the key relation, Eq. (8), wherein the fixed-nuclei GETM is averaged over the vibrational wave functions of the upper and lower electronic states. It is not necessary to make assumptions about the nature of the parametric R dependence of the GETM, but it is noted that invariance of the AN-GVOS under different kinematical conditions requires, effectively, that the FN-GEOS [Eq. (10)] exhibits a similar dependence on $\mathbf{k}_r$ and $\mathbf{k}_i$ for the range of R values in the Franck-Condon region necessary to describe the range of vibrational levels of interest.

In the calculations of this work, the GETM is treated as an R-dependent *parameter* which can be determined empirically by comparison between the calculated AN-GVOS, defined by Eq. (8), and the experimental GVOS, defined by [57,69]

$$f_{nv',0v''}(E_r,\theta)=\frac{K^2W}{2}\frac{k_i}{k_r}\sigma_{nv',0v''}(E_r,\theta), \tag{13}$$

where $\sigma_{nv',0v''}(E_r,\theta)$ is the EEL cross section for electronic-vibrational excitation. The form of Eq. (8) is particularly suitable for a study which is concerned with the relationship between optical and electron-impact excitation, as the detailed molecular physics embodied in the *unperturbed* vibrational wave functions is identical for each mode of excitation, the kinematical effects being isolated in the GETM electronic parameter which reduces to the electric-dipole transition moment in the limit of zero momentum transfer. Thus, it is possible to treat the electronic states of the molecule to any desired order of approximation, using, for example, state-of-the-art potential-energy curves determined *ab initio*, or from high-resolution optical spectra, in the determination of the vibrational wave functions. Since the primary purpose of this work is to consider the EEL spectra of electronic states which are strongly coupled, it is necessary to treat the resultant breakdown of the Born-Oppenheimer approximation *in the isolated molecule* [70]. As we shall see, this can be accomplished easily, *within the Born-Oppenheimer framework*, by considering specifically interactions between the BO molecular basis states and using the resultant coupled-channel radial wave functions in a multichannel version of Eq. (8).

All of the excited electronic states of O_2 considered in this work (7–11.2 eV) lie above the first dissociation limit at 5.21 eV and are subject to either direct dissociation or predissociation, resulting in an essentially continuous excitation cross section interspersed with predissociating resonances of varying widths. It is well known from theoretical considerations [71] that the optical oscillator-strength density df_{n0}/dW is continuous across a molecular dissociation limit and, for example, this has been verified experimentally for the Schumann-Runge system of O_2 [72]. Accordingly, Eq. (8), which is written for the case of discrete excitation, can be generalized to the case of continuous excitation via the relation [70]

$$\frac{df^{\mathrm{AN}}_{nW,0v''}(\mathbf{k}_r,\mathbf{k}_i)}{dW}=2W\left|\langle\chi_{nW}(R)|\mathcal{M}^{\mathrm{FN}}_{n0}(\mathbf{k}_r,\mathbf{k}_i;R)|\chi_{0v''}(R)\rangle\right|^2, \tag{14}$$

where $\chi_{nW}(R)$ is the *energy-normalized* radial wave function [70] for the upper state, labeled by the good quantum number W.

D. The coupled-channel method

Thus far, we have considered excitation into the vibrational levels of a single molecular electronic state. In the case of Rydberg and valence states of the same symmetry with molecular-orbital configurations differing in one or two of the occupied orbitals, such as the $^3\Pi_u$ and $^3\Sigma_u^-$ states of O_2, respectively, there may be strong interactions which invalidate the Born-Oppenheimer approximation for the isolated molecule [70]. As we have foreshadowed in Sec. III C, the breakdown of the BO approximation may be addressed by using a coupled-channel model in which the interactions between the BO basis states are included explicitly. In the adiabatic basis, the adiabatic potential-energy curves for the BO basis states exhibit an avoided crossing and these states interact nonadiabatically through an off-diagonal element of the nuclear kinetic-energy operator. In the diabatic basis, the diabatic BO basis-state potential-energy curves cross and interact through an off-diagonal element of the electrostatic Hamiltonian $\mathcal{H}^{\mathrm{el}}$. Provided that a complete electronic-state basis is employed, then the results of CC calculations are insensitive to the choice of an adiabatic or diabatic basis set. In practice, it is sufficient to include only enough interacting electronic states to describe accurately spectra in the energy region of interest. In this work, we choose the diabatic BO basis, as this has the attractive property that the wave functions, potential-energy curves, and coupling matrix elements can be expected to change smoothly with R.

The techniques of scattering theory [38,39] have been adapted to the calculation of molecular photodissociation cross sections. The CC formalism, detailed by van Dishoeck *et al.* [37] and Torop *et al.* [40], is particularly suitable for treatment of the strong Rydberg-valence interactions in O_2 and has been applied previously to explain unusual features in the optical spectrum of this molecule [35,41,42,73]. In this work, we use the CC method to obtain accurate coupled radial wave functions for the target molecule, while retaining the adiabatic-nuclei approximation in the description of the scattering process. In this approximation, the evolution of the EEL excitation spectrum from the optical limit as the momentum transfer increases is governed, essentially, only by the relative changes in the GETMs for the transitions into the interacting states.

Details of a CC formulation suitable for the description of rovibronic photodissociation of O_2 have been given by Lewis *et al.* [73]. This treatment can be extended readily to a description of electron-impact excitation. Briefly, if we neglect rotation, fine structure and degeneracy factors, the AN-GVOS density for excitation from an initial (uncoupled) electronic state Φ_0 into the m coupled states Φ_n, which include m_o open channels, is given, in matrix form, by

$$\frac{df^{\mathrm{AN}}_{W,0v''}(E_r,\theta)}{dW} = 2W\left|\langle \boldsymbol{\chi}_W(R)|\mathbf{M}^{\mathrm{FN}}(E_r,\theta;R)|\chi_{0v''}(R)\rangle\right|^2, \tag{15}$$

where $\boldsymbol{\chi}_W(R)$ is the CC diabatic radial wave-function matrix of dimension $m\times m_o$, and $\mathbf{M}^{\mathrm{FN}}(E_r,\theta;R)$ is the GETM vector of dimension $m\times 1$ with elements given by the diabatic-basis GETMs $\mathcal{M}^{\mathrm{FN}}_{n0}$. The matrix notation makes it clear that Eq. (15) is the CC analog of the single-channel Eq. (14). The CC radial wave-function matrix $\boldsymbol{\chi}_W(R)$ is the solution of the diabatic-basis CC Schrödinger equations, expressed in matrix form,

$$\left\{\mathbf{I}\frac{d^2}{dR^2} + 2\mu[W\mathbf{I}-\mathbf{V}(R)]\right\}\boldsymbol{\chi}_W(R) = \mathbf{0}, \tag{16}$$

where μ is the molecular reduced mass, $\mathbf{I}$ is the identity matrix, and $\mathbf{V}(R)$, of dimension $m\times m$, is the symmetric diabatic potential matrix. The diagonal elements of $\mathbf{V}(R)$ are the diabatic electronic potential-energy curves $V_{nn}(R) = \langle\Phi_n|\mathcal{H}^{\mathrm{el}}|\Phi_n\rangle$, and the couplings between the interacting electronic states are given by the off-diagonal elements of $\mathbf{V}(R)$, $V_{nj}(R) = \langle\Phi_n|\mathcal{H}^{\mathrm{el}}|\Phi_j\rangle$. In this work, the AN-GVOS densities calculated using Eq. (15) are compared with the experimental GVOS densities determined from EEL spectra using the continuous analog of Eq. (13) [69],

$$\frac{df_{W,0v''}(E_r,\theta)}{dW} = \frac{K^2W}{2}\frac{k_i}{k_r}\frac{d\sigma_{W,0v''}(E_r,\theta)}{dW}. \tag{17}$$

IV. RESULTS AND DISCUSSION

A. The $^3\Sigma_u^- \leftarrow X\,^3\Sigma_g^-$ transitions

The coupled-channel technique has been applied previously to gain an understanding of various aspects of the $^3\Sigma_u^- \leftarrow X\,^3\Sigma_g^-$ photoabsorption spectrum of O_2 [41,42,73]. These studies were restricted to two-state models in which only the interaction between the $\pi_u^3\pi_g^3$ valence state and the $\pi_u^4\pi_g 3p\pi_u$ Rydberg state was considered. As has been noted by Lewis *et al.* [73], two-state models provide an accurate description of the spectrum only for excitation energies $\lesssim$10.3 eV. In this work, we extend the previous CC models to include the $4p\pi_u$ Rydberg state. As we shall show, the three-state model provides a good description of the spectrum for excitation energies $\lesssim$11.2 eV, covering the region of interest.

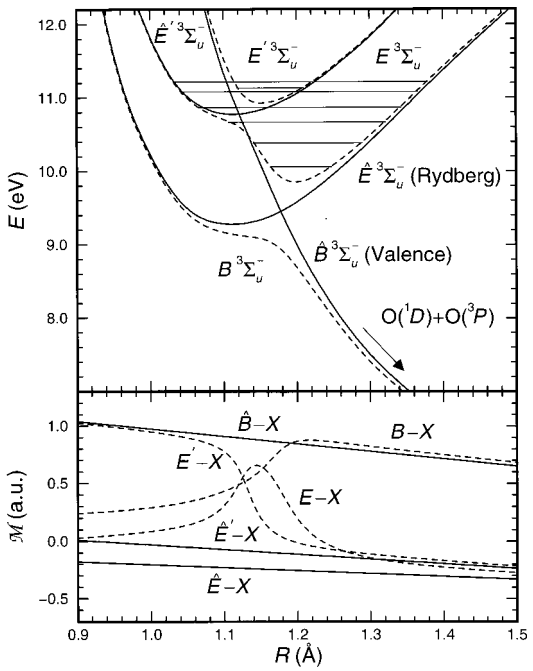

FIG. 1. Diabatic potential-energy curves and electronic transition moments (solid lines, potentials labeled $\hat{B}$, $\hat{E}$, $\hat{E}'$, in order of increasing energy for $R>1.2$ Å) used in the three-state coupled-channel calculations of the differential optical oscillator strength for the mixed Rydberg-valence $^3\Sigma_u^- \leftarrow X\,^3\Sigma_g^-$ transitions of O_2. The energy scale is referred to the minimum in the ground-state $X\,^3\Sigma_g^-$ potential-energy curve (not shown). Corresponding adiabatic potential-energy curves and electronic transition moments (dashed lines, labeled B, E, E'), determined by transformation of the diabatic quantities using the Rydberg-valence couplings in Eq. (18), are also shown. Coupled-channel energies for the upper resonances are indicated by horizontal lines, associated with the adiabatic E and E' potential-energy curves.

The diabatic potential matrix for the $^3\Sigma_u^-$ states is given by [74]

$$\mathbf{V}(R) = \begin{pmatrix} V_{\hat{B}}(R) & 0.5000 & 0.2508 \\ 0.5000 & V_{\hat{E}}(R) & 0 \\ 0.2508 & 0 & V_{\hat{E}'}(R) \end{pmatrix}, \tag{18}$$

where the diagonal elements are the diabatic potential-energy curves shown in Fig. 1, and the off-diagonal couplings are in eV. The corresponding diabatic electronic transition-moment vector is given by

$$\mathbf{M}(R)=\begin{pmatrix} \mathcal{M}_{\hat{B}X}(R) \\ \mathcal{M}_{\hat{E}X}(R) \\ \mathcal{M}_{\hat{E}'X}(R) \end{pmatrix}, \tag{19}$$

where the individual elements are also shown in Fig. 1. The potential matrix and electronic transition-moment vector were determined using a least-squares procedure in which the results of CC calculations were compared with high-resolution optical measurements for several isotopomers. Specifically, energies, predissociation linewidths, oscillator strengths, and, where possible, rotational constants associated with the $E(0)$, $E(1)$, and $E(2)$ levels [25,75], the $E(4)$ and $E(5)$ levels [76], and the $E'(0)$ level [77] were used in this iterative procedure, together with experimental $O(^1D)+O(^3P)$ photodissociation cross sections [29,30], for excitation energies from 7 to 9.8 eV, which can be associated with the $B\leftarrow X$ transition. It was assumed in deriving the CC model that the Rydberg-valence couplings were R independent, but it was necessary to assume linear R dependences for the electronic transition moments in order to reproduce correctly the relative strengths of the spectral features. The calculated cross sections were insensitive to the values of the couplings and transition moments outside the Franck-Condon region ($R\approx 1.1$–1.3 Å).

The adopted diabatic model parameters are in reasonable agreement with recent *ab initio* calculations [78] and, where comparisons are possible, are in good agreement with the results of previous two-potential CC studies [41,42,73]. It can be seen in Fig. 1 that the model diabatic potential-energy curves and electronic transition moments are physically reasonable, varying smoothly with R. Energies for the ionlike $3p\pi_u$ and $4p\pi_u$ potentials correspond to quantum defects $\delta\approx 0.8$. The fitted Rydberg-valence couplings in Eq. (18), and the diabatic Rydberg electronic transition moments in Fig. 1, at least in the Franck-Condon region, behave in reasonable agreement with the expected $(n^*)^{-3/2}$ scaling [70], where $n^*=n-\delta$ is the effective principal quantum number.

A rotationless optical CC cross section for excitation into the $^3\Sigma_u^-$ states was calculated using Eqs. (15) and (16) with the diabatic model parameters of Fig. 1 and Eqs. (18) and (19). The diabatic CC radial wave functions $\boldsymbol{\chi}_W(R)$, normalized according to the method of Mies [38], were calculated by solving Eq. (16) using the renormalized Numerov method of Johnson [79]. The ground-state vibrational wave function $\chi_{X0}(R)$ was calculated using a Rydberg-Klein-Rees potential-energy curve for the $X\,^3\Sigma_g^-$ state constructed from the spectroscopic constants of Cosby [80].

The calculated cross section is shown in Fig. 2(a), in the form of a differential optical oscillator strength, as a function of the excitation energy W. The origin of the interesting spectral features in the calculated cross section may be understood qualitatively by reference to the adiabatic potential-energy curves and electronic transition moments shown in Fig. 1, which were calculated from the corresponding diabatic parameters using the model Rydberg-valence couplings and the usual diabatic-adiabatic transformations [37]. Briefly, the broad continuum and subsidiary maxima in the 7–9.8-eV region may be associated with transitions into the

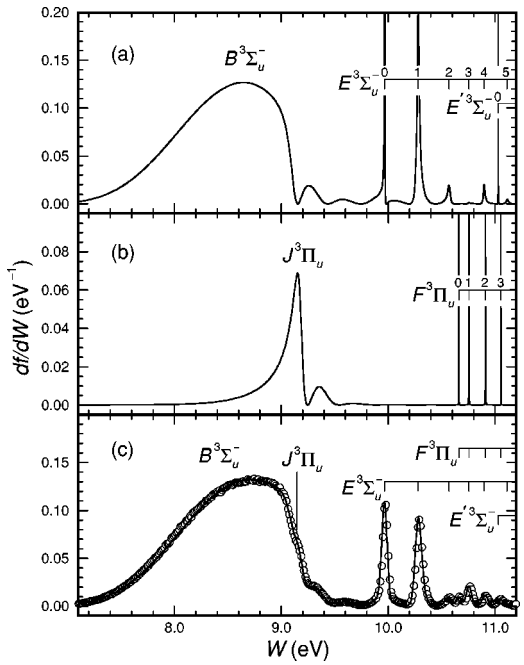

FIG. 2. (a) The rotationless differential optical oscillator strength for the mixed Rydberg-valence $^3\Sigma_u^-\leftarrow X\,^3\Sigma_g^-$ transitions of O_2, calculated using the three-state coupled-channel model of Sec. IV A with the parameters given in Fig. 1 and Eq. (18). Upper adiabatic-state assignments of the spectral features are also indicated. (b) The rotationless differential optical oscillator strength for the mixed Rydberg-valence $^3\Pi_u\leftarrow X\,^3\Sigma_g^-$ transitions, calculated using the three-state coupled-channel model of Sec. IV B with the parameters given in Fig. 3 and Eq. (20). (c) The experimental dipole (e,e) differential ''optical'' oscillator strength of Chan *et al.* [24] (open circles), compared with a rotationless coupled-channel calculation (solid line). The calculated oscillator-strength density is the sum of separate optical $^3\Sigma_u^-\leftarrow X\,^3\Sigma_g^-$ and $^3\Pi_u\leftarrow X\,^3\Sigma_g^-$ contributions [(a) + (b)], degraded with an effective instrumental resolution of 58-meV FWHM. To emphasise the good agreement between the shapes of the experimental and calculated spectra, the experimental oscillator-strength density has been lowered by 3%.

adiabatic B-state potential, the rapid decrease in the cross section near 9.1 eV being caused by the avoided crossing between the B and E states and the corresponding flattening in the B-state potential, together with the associated decrease in the adiabatic $B\leftarrow X$ electronic transition moment. Most of the predissociating resonances above 9.8 eV can be associated with the bound levels of the E-state potential which is formed by the interaction between the valence state and the $3p\pi_u$ and $4p\pi_u$ Rydberg states. The narrow resonance near 11.03 eV can be associated with the lowest level of the E' state which is the upper state formed by the interaction between the valence and $4p\pi_u$ Rydberg states [81]. It should be emphasized at this point that this adiabatic picture, while instructive, has only qualitative significance. Neither the diabatic nor the adiabatic potential-energy curves exactly represent the observed energy levels and it is necessary to employ the CC method to obtain realistic energies and cross sections. The adiabaticity parameter [82,83] for the lowest $^3\Sigma_u^-$ crossing is $\zeta\approx 1.3$, implying character intermediate be-

tween adiabatic and diabatic for the *B*- and *E*-state levels in this region.

Vibrational progressions for transitions into noninteracting Rydberg states of O_2 converging on the ground state of O_2^+ (equilibrium internuclear distance $R_e \approx 1.1$ Å) are expected to be short, since the equilibrium internuclear distance for the $X\,^3\Sigma_g^-$ state of O_2 does not differ significantly ($R_e \approx 1.2$ Å), resulting in rapidly decreasing Franck-Condon overlap factors for $v' > 2$. However, the strong Rydberg-valence interaction for the lowest $^3\Sigma_u^-$ states, which results in a considerable distortion of the *E*-state potential (Fig. 1), alters this picture. The calculated intensity distribution for the six $E \leftarrow X$ bands shown in Fig. 2(a) exhibits an interesting interference effect which can be understood qualitatively by referring to the electronic transition moments in Fig. 1. In the current model, the signs of the off-diagonal elements of the potential matrix, i.e., the Rydberg-valence couplings, are taken as positive. With this assumption, in order to correctly reproduce the experimental intensities, the $^3\Sigma_u^-$ interaction model requires that the Rydberg and valence diabatic electronic transition moments have *opposite* signs. Since the significant matrix-element product $\mathcal{M}_{\hat{B}X}(R)V_{\hat{B}\hat{E}}(R)\mathcal{M}_{\hat{E}X}(R)$ is *negative*, there is the possibility of destructive quantum interference between the Rydberg and valence transition amplitudes [70]. In fact, the *adiabatic* electronic transition moment for the $E \leftarrow X$ transition (Fig. 1) passes through zero near $R = 1.23$ Å, leading to the possibility that some vibrational bands of the $E \leftarrow X$ system may be anomalously weak. Indeed, the calculated spectrum of Fig. 2(a) shows that the (3,0) band is much less intense than either the (2,0) or (4,0) bands, providing a partial explanation for the lack of detection of the (3,0) band in any experimental spectrum.

B. The $^3\Pi_u \leftarrow X\,^3\Sigma_g^-$ transitions

The coupled-channel technique has been applied by England *et al.* [35] to a comprehensive assignment of mixed Rydberg-valence $^3\Pi_u \leftarrow X\,^3\Sigma_g^-$ bands of O_2. England *et al.* [35] employed a CC model which treated the interactions between the $\pi_u^4\pi_g\sigma_u$ valence state and the $\pi_u^4\pi_g np\sigma_u$ Rydberg states with $n = 3$–7. For consistency with our $^3\Sigma_u^-$ model of Sec. IV A, we have simplified their description [35], resulting in a three-state model sufficient to describe the spectrum accurately for excitation energies $\lesssim 11.2$ eV.

The diabatic potential matrix for the $^3\Pi_u$ states is given by

$$\mathbf{V}(R) = \begin{pmatrix} V_{\hat{J}}(R) & 0.8721 & 0.4219 \\ 0.8721 & V_{\hat{F}}(R) & 0 \\ 0.4219 & 0 & V_{\hat{F}'}(R) \end{pmatrix}, \tag{20}$$

where the diagonal elements are the diabatic potential-energy curves shown in Fig. 3, and the off-diagonal couplings are in eV. We have introduced the nomenclatures $\hat{J}$ and J to indicate the valence potential and the lowest adiabatic $^3\Pi_u$ potential, respectively. The corresponding diabatic electronic transition-moment vector is given by

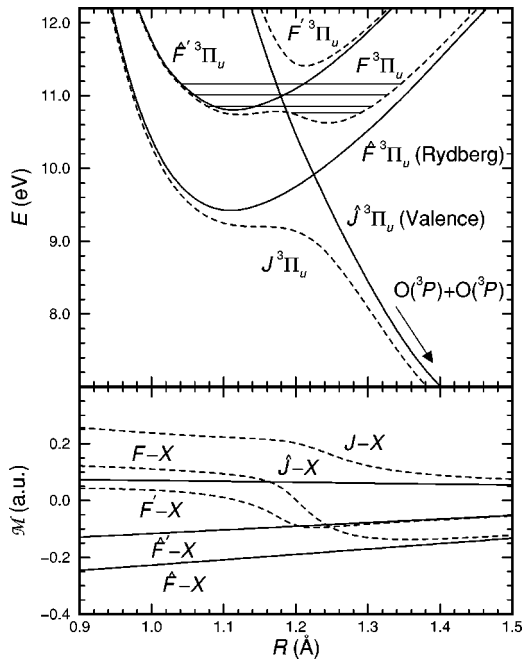

FIG. 3. Diabatic potential-energy curves and electronic transition moments (solid lines, potentials labeled $\hat{J}$, $\hat{F}$, $\hat{F}'$, in order of increasing energy for $R > 1.25$ Å) used in the three-state coupled-channel calculations of the differential optical oscillator strength for the mixed Rydberg-valence $^3\Pi_u \leftarrow X\,^3\Sigma_g^-$ transitions of O_2. The energy scale is referred to the minimum in the ground-state $X\,^3\Sigma_g^-$ potential-energy curve (not shown). Corresponding adiabatic potential-energy curves and electronic transition moments (dashed lines labeled *J*, *F*, *F*′), determined by transformation of the diabatic quantities using the Rydberg-valence couplings in Eq. (20), are also shown. Coupled-channel energies for the upper resonances are indicated by horizontal lines, associated with the adiabatic *F* potential-energy curve.

$$\mathbf{M}(R) = \begin{pmatrix} \mathcal{M}_{\hat{J}X}(R) \\ \mathcal{M}_{\hat{F}X}(R) \\ \mathcal{M}_{\hat{F}'X}(R) \end{pmatrix}, \tag{21}$$

where the individual elements are shown in Fig. 3. Data used to optimize the diabatic model parameters included energies, rotational constants, predissociation linewidths, and oscillator strengths associated with the $F(0)$, $F(1)$, $F(2)$, and $F(3)$ levels [35], together with experimental $O(^3P) + O(^3P)$ photodissociation cross sections [29,30] which can be associated with the $J \leftarrow X$ transition.

Most of the comments made in Sec. IV A regarding the $^3\Sigma_u^-$ Rydberg-valence interaction can be applied equally to the $^3\Pi_u$ interaction and will not be repeated here. However, there are two differences of degree which should be noted. First, whereas the principal molecular-orbital configurations of the $^3\Sigma_u^-$ valence and Rydberg states differ in two of the occupied orbitals, in the case of the $^3\Pi_u$ states the difference is only one orbital. This implies a stronger Rydberg-valence coupling (0.87 eV for the $n = 3$ interaction, compared with 0.50 eV for the $^3\Sigma_u^-$ case) which results in a much more strongly avoided crossing and the repulsion of the *F*-state

levels to significantly higher energies than the *E*-state levels. Second, whereas the diabatic Rydberg electronic transition moments in the Franck-Condon region are of similar magnitudes for both symmetries, the valence moment for the $^3\Pi_u$ symmetry is more than an order of magnitude smaller than the corresponding moment for the $^3\Sigma_u^-$ symmetry. This latter result is consistent with *ab initio* calculations [28,33].

The consequences of these differences are evident in the calculated rotationless CC cross section for excitation into the $^3\Pi_u$ states, which is shown in Fig. 2(b). Because of the small valence electronic transition moment, there is no strong continuum. The $J \leftarrow X$ features are confined to a narrow energy region near 9.15 eV and are associated with the flattening of the *J*-state potential produced by the strongly avoided crossing with the *F* state. As has been discussed fully by England *et al.* [35], the irregular vibrational structure of the *F* state arises essentially from the double-minimum nature of the *F*-state potential which is formed by strong interactions between the valence state and the $3p\sigma_u$ and $4p\sigma_u$ Rydberg states.

The adiabaticity parameter for the lowest $^3\Pi_u$ crossing is $\zeta \approx 2.9$, implying character tending towards adiabatic for the *J*- and *F*-state levels in this region. In the adiabatic picture, the predissociation broadening of the *F*-state levels is caused by coupling of the adiabatic *F* state to the repulsive adiabatic *J* state (Fig. 3) through nonadiabatic interactions. Higher values for the adiabaticity parameter imply smaller nonadiabatic coupling and, hence, a smaller probability of predissociation. This explains qualitatively why the *F*-state levels shown in Fig. 2(b) are significantly narrower than the *E*-state levels shown in Fig. 2(a).

Although there are no large interference effects evident in the calculated vibrational intensity distribution for the $F \leftarrow X$ bands, it is clear from the model electronic transition moments shown in Fig. 3 that such a possibility exists. As for the $^3\Sigma_u^-$ case, in order to explain the observed intensities it is necessary that the matrix-element product $\mathcal{M}_{\hat{J}X}(R)V_{\hat{J}\hat{F}}(R)\mathcal{M}_{\hat{F}X}(R)$ is *negative*. As a consequence, the adiabatic electronic transition moment for the $F \leftarrow X$ transition passes through zero near $R = 1.20$ Å, leading to the possibilty of destructive interference effects controlling the intensities for some of the $F \leftarrow X$ bands.

C. The optical spectrum

It is of interest to compare the calculated optical CC spectra for the electric-dipole-allowed transitions of O_2 with electron energy-loss spectra taken under conditions of vanishing momentum transfer. Geiger and Schröder [16] measured a very-high-resolution EEL spectrum of O_2 in the 6.8–21-eV energy-loss range, taken with an impact energy of 25 keV and small scattering angle, but only relative intensities, rather than absolute oscillator strengths, were reported. Huebner *et al.* [45] reported oscillator strengths in the 6–14-eV energy-loss range, derived from EEL measurements taken with an impact energy of 100 eV and a small scattering angle, but these results must be regarded as doubtful since the momentum transfer was too large for the optical limit to apply [24]. More recently, Chan *et al.* [24] have reported absolute oscillator strengths in the 5–30-eV energy-loss range, derived from EEL spectra measured with an impact energy of 3 keV, a mean scattering angle $\theta = 0°$, and an instrumental resolution of 48-meV FWHM. The momentum transfer applying to these dipole (e,e) spectra was sufficiently low for the optical limit to be valid. Chan *et al.* [24] converted their EEL spectra into differential oscillator strength spectra using a modified version of Eq. (13) which included careful allowance for the effects of limited instrumental angular resolution about the 0° scattering angle. Their oscillator strengths were calibrated in the 26-eV energy-loss region against earlier low-resolution dipole (e,e) spectra [46] which had been normalized using procedures based on the Thomas-Reiche-Kuhn sum rule [46].

The differential ''optical'' oscillator-strength spectrum determined by Chan *et al.* [24] is compared in Fig. 2(c) with our calculated CC spectrum. The CC spectrum is simply the sum of the rotationless CC spectra for the $^3\Sigma_u^- \leftarrow X\,^3\Sigma_g^-$ and $^3\Pi_u \leftarrow X\,^3\Sigma_g^-$ transitions, given in Figs. 2(a) and 2(b), respectively, following convolution with a Gaussian function of 58-meV FWHM. The experimental spectrum has been lowered by 3% to emphasize the excellent agreement between the shapes of the calculated and measured spectra. Differences between the spectra are insignificant. First, the relatively small discrepancy between the 48-meV FWHM instrumental resolution quoted by Chan *et al.* [24] and the 58-meV FWHM resolution used by us to optimize the agreement for the sharp peaks can be explained, at least in part, by the neglect of rotational structure and fine structure in the CC calculations. Second, the ~10 meV discrepancy between the energy scales evident from an inspection of the peaks in the 10–11 eV energy-loss region, which is, in any case, small compared with the instrumental resolution, can be understood by noting that the experimental energy scale was calibrated only against a He transition at 21.218 eV energy loss [84]. Third, the 3% discrepancy between the experimental and CC oscillator strengths in the ~9-eV energy-loss region is within the combined uncertainties [85] and is a testament to the reliability of the Bethe-Born factor employed by Chan *et al.* [24], since their intensity calibration point is at 26-eV energy loss.

Two conclusions follow from the excellent agreement between the experimental and calculated spectra of Fig. 2(c). First, notwithstanding a limited instrumental resolution, the claim by Chan *et al.* [24] to have measured an absolute ''optical'' spectrum has been verified, since the CC spectrum is based on a fit to very high-resolution absolute optical cross sections. Second, we have shown that a coupled-channel model based on three-state treatments of the Rydberg-valence interactions for the $^3\Sigma_u^-$ and $^3\Pi_u$ states explains all spectral features in the 7–11.2 eV energy-loss range *quantitatively*. Clearly, the bulk of the observed oscillator strength arises from the $^3\Sigma_u^- \leftarrow X\,^3\Sigma_g^-$ transitions, with the lowest-energy $J\,^3\Pi_u \leftarrow X\,^3\Sigma_g^-$ feature appearing only as an inflection on the high-energy side of the $B \leftarrow X$ continuum. The first four peaks in the high energy-loss region, i.e., the longest, second, and third bands and the $F(0) \leftarrow X$ band, are single, while the four discernible peaks at higher energy loss

consist of overlapping transitions involving the E, E', and F states. The assignments in Fig. 2(c) correct those of Buenker *et al.* [21], repeated by Chan *et al.* [24], which were in error for the $F \leftarrow X$ transitions.

D. EEL spectra at intermediate impact energies

In this section we extend the coupled-channel treatment to a description of EEL spectra for impact energies where the optical limit is inapplicable. This is achieved by retaining the CC models detailed in Secs. IV A and IV B to describe the structure of the mixed Rydberg-valence states of the O_2 target molecule, but allowing the elements of the electronic transition moment vector to vary. This approach is consistent both with the philosophy of the generalized electronic transition moment espoused in Sec. III and the general FBA formalism of Dillon *et al.* [17].

The relative intensities of vibrational features arising from transitions into Rydberg-valence coupled states of a given symmetry depend essentially on the *ratio* of the Rydberg and valence GETMs. For simplicity, we consider only that parameter space in which the relative R dependences of the relevant elements of the GETMs remain constant, and in which the $n=3$ and $n=4$ Rydberg GETMs are scaled by a common factor relative to the valence GETM. In this case, we can define a single dimensionless parameter

$$r=(\mathcal{M}_{\mathrm{R}}/\mathcal{M}_{\mathrm{v}})/(\mathcal{M}_{\mathrm{R}}/\mathcal{M}_{\mathrm{v}})_{\mathrm{opt}}, \tag{22}$$

where the subscripts R and v indicate the $(n=3)$ Rydberg and valence moments, respectively, in terms of which the relative intensities computed using the CC technique may be described. As implied by Eq. (22), values of this parameter for each symmetry, r_Σ and r_Π, are normalized using the optical-limit moments given in Secs. IV A and IV B for the $^3\Sigma_u^-$ and $^3\Pi_u$ states, respectively.

In Fig. 4(a), the results of CC calculations of the relative intensities of the $^3\Sigma_u^- \leftarrow X\,^3\Sigma_g^-$ EEL features are presented for a wide range of transition-moment ratios r_Σ, with all values given relative to the intensity of the longest band $E \leftarrow X(0,0)$ [86]. It is evident from Fig. 4(a) that allowing the transition-moment ratio to vary from the optical value, achievable experimentally through, e.g., the employment of electron-impact excitation, allows a rich range of behaviors of the relative intensities to be accessed. Rapid changes in the relative intensities occur, especially near the intensity minima occurring for particular resonances as the destructive quantum-interference effects vary with r_Σ. Similar comments apply to the CC calculations of relative intensities for the $^3\Pi_u \leftarrow X\,^3\Sigma_g^-$ transitions, shown in Fig. 4(b) relative to the $F \leftarrow X(0,0)$ intensity [86]. However, in this case the interesting region of most rapid change occurs for $r_\Pi < 1$, rather than $r_\Sigma > 1$ in Fig. 4(a). This difference in behavior occurs because of the vastly different optical transition-moment ratios for the two symmetries [see Figs. 1 and 3; the optical $(n=3)$ Rydberg:valence ratios are approximately 0.3 and 3, for the $^3\Sigma_u^-$ and $^3\Pi_u$ states, respectively, near $R = 1.2$ Å].

In Fig. 5(a), computed oscillator-strength densities for the optically allowed transitions of O_2 are presented for selected combinations of r_Σ, r_Π, and $\Sigma{:}\Pi$ weights, chosen so as to optimize overall relative agreement with the experimental oscillator-strength densities summarized in Fig. 5(b) for various non-FBA scattering conditions. The experimental oscillator-strength densities were derived using Eq. (17) from the EEL spectra measured here and in Ref. [4]. The computed densities, obtained using Eq. (15), are the sums of separate rotationless CC calculations for the $^3\Sigma_u^- \leftarrow X\,^3\Sigma_g^-$ and $^3\Pi_u \leftarrow X\,^3\Sigma_g^-$ transitions, degraded by convolution with a Gaussian function of 30-meV FWHM to account for the effects of limited instrumental resolution and broadening due to the neglected rotational and fine structure. Both the computed and experimental spectra in Fig. 5 are normalized to the same constant integrated intensity for the longest band. Under all conditions, the experimental spectra are contaminated by the effects of electric-dipole-forbidden transitions, particularly the $g \leftarrow g$ transitions into the $3s$, $4s$, and $3d$ Rydberg states, indicated on Fig. 5(b). Nevertheless, it is clear that many features arising from the optically allowed transitions vary markedly in relative intensity as the scattering conditions are varied. In particular, for the case of transitions into the $^3\Sigma_u^-$ states, intensities of both the SR continuum $B \leftarrow X$ and the second band $E \leftarrow X(1,0)$ decrease rapidly with respect to that of the longest band $E \leftarrow X(0,0)$ as the momentum transfer increases. In the case of the $^3\Pi_u$ states, under the same conditions the relative intensity of the $F \leftarrow X(0,0)$ transition at 10.66 eV at first decreases rapidly from the optical value [see Fig. 2(c)], then passes through a

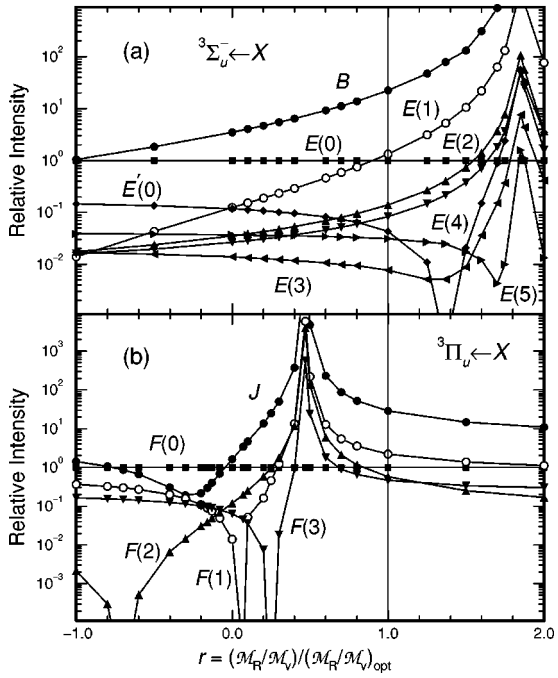

FIG. 4. Variation in the relative intensities of vibrational features in the optically allowed electronic transitions of O_2 calculated using the coupled-channel method, as the ratio of the Rydberg and valence generalized electronic transition moments is changed from the optical value. (a) The $^3\Sigma_u^- \leftarrow X\,^3\Sigma_g^-$ transitions as a function of r_Σ. (b) The $^3\Pi_u \leftarrow X\,^3\Sigma_g^-$ transitions as a function of r_Π.

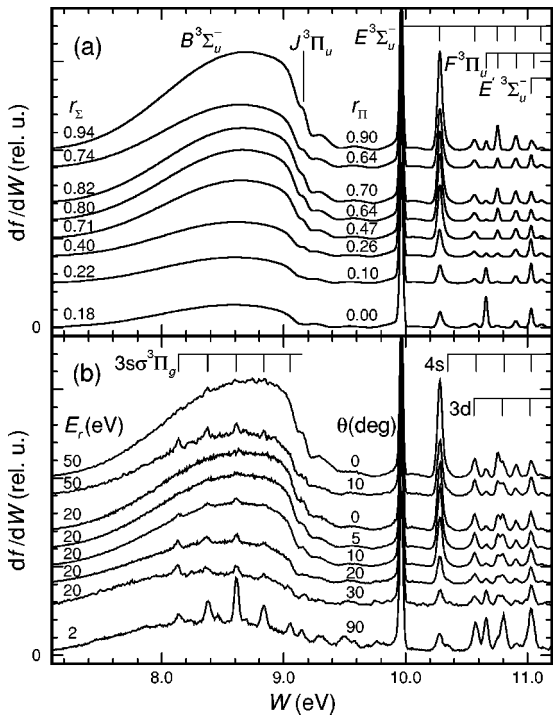

FIG. 5. Comparison between experimental and modeled electron energy-loss spectra for O_2 in the 7.1–11.2-eV energy-loss region. All spectra have been normalized to a constant integrated intensity for the longest-band peak at 9.97 eV. (a) Summed oscillator-strength densities for the optically allowed transitions, $^3\Sigma_u^- \leftarrow X\,^3\Sigma_g^-$ and $^3\Pi_u \leftarrow X\,^3\Sigma_g^-$, calculated using the coupled-channel method, with indicated parameters r_Σ and r_Π optimized by overall comparison with the experimental spectra. The computed spectra have been convolved with a Gaussian instrumental function of 30-meV FWHM. (b) Experimental oscillator-strength densities for various indicated scattering conditions. In addition to the optically allowed transitions, all experimental spectra contain features arising from optically forbidden transitions, especially the $g \leftarrow g$ transitions into the indicated $3s$, $4s$, and $3d$ Rydberg states.

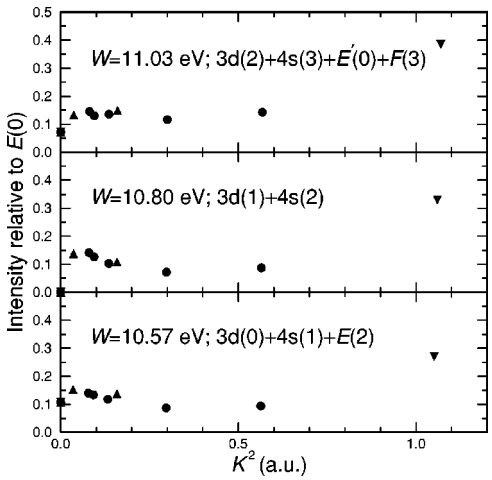

FIG. 6. Experimental intensities as a function of K^2, relative to the longest band [labeled $E(0)$], for the energy-loss peaks at $W = 10.57$, 10.80, and 11.03 eV, which contain partial or total contributions from optically forbidden transitions into the $3d(v)$ and $4s(v+1)$ Rydberg levels. Circles: $E_r = 20$ eV. Upward triangles: $E_r = 50$ eV. Downward triangles: $E_r = 2$ eV.

minimum, and finally increases rapidly. Two points are worthy of note following a comparison between Figs. 5(a) and 5(b). First, the general behavior of the relative experimental intensities for the optically allowed transitions is reproduced in the computed spectra. Second, the values of r_Σ and r_Π necessary to achieve this agreement decrease from unity towards zero as the momentum transfer increases, in quite similar ways for each symmetry.

In order to establish the detailed behavior of the optically allowed EEL peaks in Fig. 5(b), it is necessary to make allowances for the contributions of optically forbidden transitions. In Fig. 6, the relative intensities of three peaks at 10.57, 10.80, and 11.03 eV, deduced from the experimental spectra of Fig. 5(b) and plotted as a function of K^2, are seen to exhibit somewhat similar behavior, with rapid initial increases in relative intensity, followed by gentle decreases, and finally strong increases, as K^2 increases. These peaks are very prominent in the $E_r = 2$ eV, $\theta = 90°$ spectrum and coincide with the known energies of transitions into vibrational levels of $3d$ and $4s$ Rydberg states of various symmetries [87]. The $K^2 = 0$ points in Fig. 6 were deduced from various high-resolution optical oscillator-strength measurements [25,35,75,77]. The 10.80-eV peak is unique in corresponding purely to an optically forbidden transition. We assume that it corresponds principally to $3d \leftarrow X(1,0)$ and $4s \leftarrow X(2,0)$ transitions [88]. Adopting the additional assumption that the contributions of other vibrational levels of the $3d,4s \leftarrow X$ systems to the peaks at 10.57 and 11.03 eV have the same K^2 dependences as that for the 10.80-eV peak, we have corrected the relative intensities of the 10.57 and 11.03 eV peaks for the effects of the optically forbidden transitions. This was achieved by applying scaling factors to the 10.80-eV intensity of 0.7 and 0.8, respectively [89].

In Fig. 7, intensities of all accessible EEL peaks arising from $^3\Sigma_u^- \leftarrow X\,^3\Sigma_g^-$ transitions are plotted as a function of K^2 and compared with intensities computed using the CC method, plotted as a function of $1 - r_\Sigma$. Both the experimental and computed intensities are given relative to that of the longest band $E \leftarrow X(0,0)$. The experimental intensities have been derived from the spectra in Fig. 5(b) [90], with $K^2 = 0$ values obtained from various optical spectra and oscillator-strength measurements [24,25,75,77,91]. The $E \leftarrow X(2,0)$ and $E' \leftarrow X(0,0)$ intensities in Fig. 7 have been corrected for the effects of optically forbidden transitions, as described in the previous paragraph. In addition, the $E \leftarrow X(4,0)$ and $E' \leftarrow X(0,0)$ intensities have been corrected for the effects of weaker $F \leftarrow X$ transitions [92]. ''Structures'' observed at low K^2 values in the experimental $E \leftarrow X(2,0)$ and $E' \leftarrow X(0,0)$ intensities in Fig. 7 are probably artifacts related to inadequacies in the correction process for the optically forbidden contributions.

Overall, relative to the intensity of the longest band, intensities of the EEL features arising from the Rydberg-valence mixed $^3\Sigma_u^- \leftarrow X\,^3\Sigma_g^-$ transitions illustrated in Fig. 7 exhibit a wide range of non-Franck-Condon behavior as K^2 increases, ranging from a large decrease for the second band $E \leftarrow X(1,0)$, through a small decrease for $E \leftarrow X(5,0)$, to a

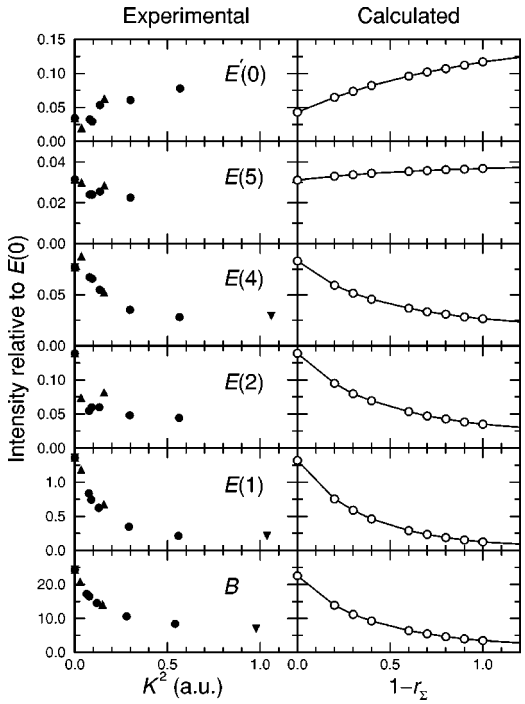

FIG. 7. Comparison between the experimental and model behavior of the relative intensities of energy-loss features associated with transitions into the mixed Rydberg-valence $^3\Sigma_u^-$ states of O_2, for a range of scattering conditions. All results have been normalized to the integrated intensity of the longest band [labeled $E(0)$], and the experimental results for $E(2)$, $E(4)$, and $E'(0)$ have been corrected for the effects of overlapping transitions. The experimental intensities, plotted as a function of K^2 (circles: $E_r=20$ eV; upward triangles: $E_r=50$ eV; downward triangles: $E_r=2$ eV), correlate with the model calculations, plotted as a fuction of $1-r_\Sigma$.

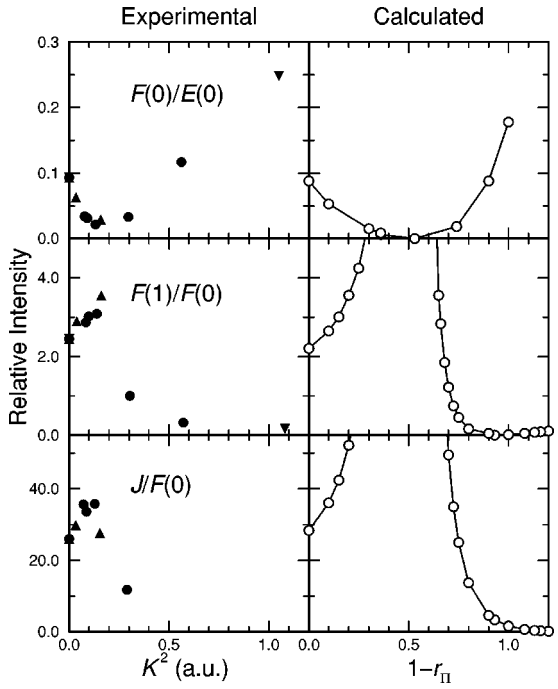

FIG. 8. Comparison between experimental and model behavior of the relative intensities of energy-loss features associated with transitions into the mixed Rydberg-valence $^3\Pi_u$ states of O_2, normalized to the peak at 10.66 eV [labeled $F(0)$], for a range of scattering conditions. The contrasting behavior of the transitions into the $F\,^3\Pi_u(0)$ and $E\,^3\Sigma_u^-(0)$ states is also shown in the upper panels. The experimental intensities, plotted as a function of K^2 (circles: $E_r=20$ eV; upward triangles: $E_r=50$ eV; downward triangles: $E_r=2$ eV), correlate with the model calculations, plotted as a function of $1-r_\Pi$.

significant increase for $E'\leftarrow X(0,0)$. Thus, the unusual persistency of the longest band under all scattering conditions is not unique, being nearly matched by $E\leftarrow X(5,0)$ and exceeded by $E'\leftarrow X(0,0)$. While there is a small, systematic dependence of the experimental relative intensities on E_r, as might be expected under non-FBA conditions, with, e.g., the 50 eV values generally exceeding the 20 eV values, this energy dependence is dwarfed by the major variations caused by the Rydberg-valence interactions discussed here. Remarkably, the behavior of the computed relative intensities in Fig. 7 matches the experimental behavior in detail for all features, with the exception of $E\leftarrow X(5,0)$ where the experimental values decrease slightly as K^2 increases, while the computed values increase slightly as $1-r_\Sigma$ increases. Overall, these results provide convincing evidence for the validity of our coupled-channel generalized-electronic-transition-moment treatment, suggesting a loose correspondence between K^2 and $1-r_\Sigma$. For example, if a value for $1-r_\Sigma$ is deduced from Fig. 7 by equating the experimental and theoretical relative intensities for, say, $E\leftarrow X(1,0)$, then the relative intensities computed with the *same value* of $1-r_\Sigma$ provide decent descriptions of the experimental behavior *for all other bands*.

Unfortunately, the comparative weakness of the $^3\Pi_u\leftarrow X\,^3\Sigma_g^-$ systems of O_2 makes them difficult to study, but it is possible to obtain useful intensity information on the lower levels from the EEL spectra of Fig. 5(b). In Fig. 8 (lower panels), experimental intensities for the $J\leftarrow X$ and $F\leftarrow X(1,0)$ bands [93], relative to that for $F\leftarrow X(0,0)$, are plotted as a function of K^2 and compared with corresponding CC calculations, plotted as a function of $1-r_\Pi$. The $K^2=0$ points were obtained from experimental optical oscillator-strengths [30,35], and the $F\leftarrow X(1,0)$ intensities have undergone a small computed correction for the effects of the weak $E\leftarrow X(3,0)$ band. Both the $J\leftarrow X$ and $F\leftarrow X(1,0)$ experimental relative intensities in Fig. 8 rise to a maximum and then fall off rapidly as K^2 increases, behavior quite different from that observed for the corresponding $^3\Sigma_u^-\leftarrow X\,^3\Sigma_g^-$ transitions. Nevertheless, this observed behavior is reproduced qualitatively by the computed intensities, indicating a loose correlation between K^2 and $1-r_\Pi$. In Fig. 8 (upper panel), it can be seen clearly that the experimental $F\leftarrow X(0,0)$ intensity goes through a deep minimum relative to the $E\leftarrow X(0,0)$ intensity at quite a small value of K^2, a behavior confirmed by additional angular-dependence measurements (not shown). While this behavior is reproduced by the calculations [94], the fact that the experimental minimum intensity ratio is clearly nonzero (~ 0.02), compared with a near-zero computed value, leads to the significant quantita-

tive differences between the experimental and computed $^3\Pi_u \leftarrow X\,^3\Sigma_g^-$ intensity ratios in Fig. 8.

It is of importance to consider the possible causes of the nonzero minimum in the $F \leftarrow X(0,0)$ relative intensity. The most obvious explanation would involve the presence of a coincident optically forbidden transition to another electronic state which contaminates the measurements of the pure $F \leftarrow X(0,0)$ transition. We believe that this explanation is unlikely for the following reasons. First, the $F \leftarrow X(0,0)$ EEL peak at 10.66 eV is well separated from vibrational features due to the $3d,4s \leftarrow X$ systems discussed above [87]. Thus, $g \leftarrow g$ optically forbidden transitions cannot be playing a role. Second, perusal of available information on the $3p\sigma_u$ and $3p\pi_u$ Rydberg states of O_2 shows only two states in the vicinity of $F(0)$ which can contribute to optically forbidden $u \leftarrow g$ transitions [95], specifically, a $^1\Delta_u$ level centered on 10.63 eV energy loss, with a FWHM of ~ 0.1 eV [96], and a $^3\Delta_u$ level at 10.64 eV [96]. These levels are sufficiently well separated from $F(0)$ to be excluded as possible contributors to the intensity of the 10.66-eV peak which retains position and shape under all scattering conditions. Therefore, it appears that the experimental behavior of the 10.66-eV peak reflects only the behavior of the $F \leftarrow X(0,0)$ transition, leading us to question the theoretical prediction of a near-zero minimum in intensity. We have performed additional calculations for finite temperatures which include all optically allowed fine-structure components and the effects of limited experimental angular resolution, but these do not materially alter the theoretical result. We believe that the answer to the dilemma involves the spin structure of the upper and lower levels in the $F\,^3\Pi_u \leftarrow X\,^3\Sigma_g^-$ transition. The $^3\Sigma_g^-$ state has $|\Omega| = 0,1$, while the $^3\Pi_u$ state has $|\Omega| = 0,1,2$, with only the perpendicular subtransitions $1 \leftarrow 0$ and $2,0 \leftarrow 1$ being electric dipole allowed. Therefore, our explanation involves suggesting that the optically forbidden subtransitions $0,2 \leftarrow 0$ and/or $1 \leftarrow 1$ become allowed under conditions of electron-impact excitation, thus contributing to the intensity of the 10.66-eV EEL peak. Since these subtransitions do not connect the same fine-structure levels as the optically allowed subtransitions, no additional interference effects occur and their intensities would add incoherently to the intensities of the allowed subtransitions, which, themselves, are not precluded from passing through a near-zero intensity minimum, as predicted by our calculations. This explanation leads to an interesting prediction. If the transition of interest were an optically allowed singlet-singlet transition, then the above fine-structure considerations would not apply, and, in similar circumstances of Rydberg-valence mixing, the destructive interference effects might well result in the observation of a near-zero minimum in intensity in the EEL spectra, with the complete disappearance of a band under specific scattering conditions.

Overall, the results presented above indicate that a diabatic mixed-state description of the molecule, coupled with a generalization of the GETM picture beyond the realm of the FBA, together give a good description of the many irregularities in the relative intensities of mixed Rydberg-valence transitions in EEL spectra, suggesting a correlation between

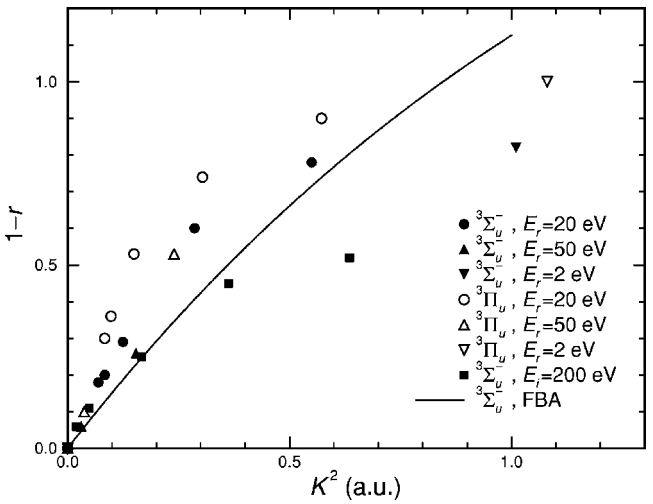

FIG. 9. Relationships between $1-r$ and K^2 for the mixed Rydberg-valence $^3\Sigma_u^- \leftarrow X\,^3\Sigma_g^-$ (solid symbols) and $^3\Pi_u \leftarrow X\,^3\Sigma_g^-$ (open symbols) transitions of O_2, determined empirically using the computed and experimental EEL spectra of Fig. 5. Results deduced from the experimental second-band:longest-band intensity ratios of Dillon *et al.* [17] at $E_i = 200$ eV, through comparison with the computed ratios of this work [Fig. 4(a)] are also shown (solid squares), as are their *ab initio* results [17,97] for the $^3\Sigma_u^- \leftarrow X\,^3\Sigma_g^-$ transitions, calculated within the first Born approximation (solid line).

the square of the experimental momentum transfer and $1-r$, where r is as defined in Eq. (22). In Fig. 9, relationships between $1-r$ and K^2 are presented for the $^3\Sigma_u^- \leftarrow X\,^3\Sigma_g^-$ and $^3\Pi_u \leftarrow X\,^3\Sigma_g^-$ Rydberg-valence transitions of O_2. These relationships were determined empirically using the best-fit-computed and experimental EEL spectra of Fig. 5. Also shown in Fig. 9 are empirical results for the $^3\Sigma_u^- \leftarrow X\,^3\Sigma_g^-$ transitions deduced using second-band:longest-band intensity ratios from the $E_i = 200$-eV EEL spectra of Dillon *et al.* [17] and our computations of Fig. 4(a), together with fully theoretical results implied by their [17,97] *ab initio* calculations of the diabatic GETMs within the FBA [98]. The present results for both the $^3\Sigma_u^- \leftarrow X\,^3\Sigma_g^-$ and $^3\Pi_u \leftarrow X\,^3\Sigma_g^-$ transitions in Fig. 9 show a rapid linear dependence of $1-r$ on K^2, for small K^2, followed by a degree of ''saturation'' at higher K^2. The initial slopes are discernibly larger for $E_r = 20$ eV than for $E_r = 50$ eV, and are also larger for the $^3\Pi_u \leftarrow X\,^3\Sigma_g^-$ transitions than for the $^3\Sigma_u^- \leftarrow X\,^3\Sigma_g^-$ transitions. Similar behavior is observed for the $E_i = 200$ eV results of Dillon *et al.* [17] for the $^3\Sigma_u^- \leftarrow X\,^3\Sigma_g^-$ transitions, albeit with an earlier onset of saturation which acts to limit the accessible ranges of $1-r$ and the corresponding intensity ratios. The *ab initio* results for the $^3\Sigma_u^- \leftarrow X\,^3\Sigma_g^-$ transitions in the case of the FBA [17,97] show reasonable agreement with the $E_i = 200$ eV measurements, but a much lesser degree of saturation.

Our results imply that relative intensities of vibrational features for mixed Rydberg-valence transitions in EEL spectra provide a sensitive probe of the relative Rydberg and

valence GETMs, and that, relative to the valence GETM, the Rydberg GETM decreases rapidly as K^2 increases. This conclusion is consistent with the *ab initio* calculations of Dillon *et al.* [17,97] which show, for the $^3\Sigma_u^- \leftarrow X\,^3\Sigma_g^-$ transitions within the FBA, that the magnitude of the diabatic $(n=3)$ Rydberg GETM at $R=2.3$ a.u. decreases to zero near $K^2=0.85$ a.u., while the valence GETM decreases only by $\sim 30\%$. Considering the diffuse nature of the Rydberg orbitals and a likely correspondingly increased sensitivity to the influence of the impacting electron, such a result can be easily understood. Notwithstanding small systematic differences between the results in Fig. 9 for the $^3\Sigma_u^- \leftarrow X\,^3\Sigma_g^-$ and $^3\Pi_u \leftarrow X\,^3\Sigma_g^-$ transitions, essentially similar GETM behavior is observed for both transitions. This is a remarkable result, given the order-of-magnitude difference in the Rydberg:valence optical-limit electronic transition-moment ratios, and implies that the $np\pi_u\,^3\Sigma_u^- \leftarrow X\,^3\Sigma_g^-$ and $np\sigma_u\,^3\Pi_u \leftarrow X\,^3\Sigma_g^-$ Rydberg GETMs evolve in similar ways as the scattering conditions are altered.

Finally, we recall some of the approximations and assumptions underlying our analysis. First, in the specific coupled-channel analyses described in this section, for clarity we have made simple assumptions regarding the R and n^* dependences of the GETMs. While relaxation of these constraints in the CC model certainly results in improved quantitative agreement with experiment, these improvements are in detail only, and the principal conclusions of this section are unaltered. Second, the value of residual energy below which the fundamental adiabatic-nuclei approximation employed in this work becomes invalid is unclear [99], as is the value of E_r below which the GETMs become *effective* (see Sec. III B). Third, we have assumed nonresonant scattering. Intensity anomalies due to the effects of negative-ion resonances may well play a role at low impact energies [100], but here we consider only those effects arising from the evolving GETMs of the interacting molecular electronic states. Further theoretical work addressing these latter points would be valuable.

E. Spectral decomposition

As one of the fundamental steps in extracting cross-section information from EEL spectra, least-squares-fit deconvolution techniques are typically employed [3] in the analysis of overlapping vibrational progressions. In this procedure, several assumptions are made. First, the energies for each of the vibrational levels of the electronic states of interest, relative to the $v''=0$ level of the ground electronic state, are assumed known. Second, the respective Franck-Condon factors for the pertinent transitions are also assumed to be known, and, third, the instrumental function is assumed to be Gaussian in form. Finally, and perhaps most importantly, each of these criteria is assumed to hold irrespective of the kinematical conditions. These techniques have been employed successfully in studies on electron-impact excitation of the electronic states of N_2 [5] and the metastable $a^1\Delta_g$ and $b^1\Sigma_g^+$ states of O_2 [4,6]. While the various electronic states in these studies were overlapped in energy loss, there were no strong perturbative interactions between the states and the usual assumptions listed above remained valid. In addition, several attempts have been made to decompose the EEL spectra of overlapping electronic states excited into the continuous regions of their spectra. These analyses assumed that the continuous spectrum of each contributing electronic state could be represented by a broad Gaussian profile [53,59]. As will be described in more detail below, the results of the previous sections show clearly that some of the assumptions underlying these techniques for the deconvolution of overlapping discrete or continuous spectra are completely invalid in the case of transitions into excited states of strongly mixed character, e.g., the Rydberg-valence states of O_2.

In the case of the $E \leftarrow X$ transition of O_2, which is of heavily mixed Rydberg-valence character, the present EEL results, together with those of Dillon *et al.* [17], show that the intensity of the (1,0) band decreases much faster than the intensity of the (0,0) band as the impact energy decreases (or the scattering angle increases). In fact, due to the anomalous behavior of these bands, it was not realized that they were members of a vibrational progression until this was suggested by optical and theoretical studies [18,19,21,26,101]. York and Comer [2], for example, suggested that the strong relative intensity of the (0,0) band, under conditions of low impact energy and high scattering angle, might indicate the presence of an electric-dipole-forbidden transition at the same energy-loss location. Clearly, if the invariance of vibrational intensities under different scattering conditions is invoked to decompose overlapping vibrational progressions involving strongly mixed states, such as the $E^3\Sigma_u^-$ state of O_2, then the resultant decomposition will be invalid.

Cartwright *et al.* [59] and Shyn *et al.* [53] have attempted to decompose the Schumann-Runge continuum region of the O_2 spectrum into contributions from transitions to different electronic states. They employed similar models in which each contribution to the diffuse spectrum was assumed to have a Gaussian shape and the number, positions, widths, and intensities of these Gaussians were adjusted to fit the observed EEL spectra. Cartwright *et al.* [59] analyzed the 25-keV, 0° spectrum of Geiger and Schröder [16], together with 12 spectra taken at impact energies of 20, 30, and 45 eV. Ignoring the small, discrete contributions of Rydberg states in the 7–9.5-eV energy-loss region, they [59] found that transitions into four valence states with vertical excitation energies of 7.50, 8.30, 8.68, and 8.93 eV were necessary to explain fully all of their EEL spectra. The weak 7.5-eV peak was attributed to an electric-dipole-forbidden transition into a $^3\Pi_g$ state, the 8.30- and 8.68-eV peaks to electric-dipole-allowed transitions into the $B^3\Sigma_u^-$ and $^3\Pi_u$ states, respectively, and the 8.93-eV peak to an unknown transition. Shyn *et al.* [53] analyzed 338 spectra covering the impact-energy range 15–50 eV and the scattering-angle range 12°–156° and found that their spectra could be reproduced using only three broad Gaussians, corresponding to transitions into valence states with vertical excitation energies of 7.65, 8.34, and 8.87 eV, assigned as the $^3\Pi_g$, $B^3\Sigma_u^-$ and an unknown state, respectively. Each group of investigators [53,59] attempted to determine potential-energy curves for

the valence states excited in the Schumann-Runge region by inverting their results, assuming linear potentials in the Franck-Condon region and what were, effectively, *R*-independent GETMs for the excitations.

Our coupled-channel results show clearly that the assumptions underlying the spectral decompositions of Cartwright *et al.* [59] and Shyn *et al.* [53] are invalid. It is certainly true that the main feature in the Schumann-Runge continuum region is due to the electric-dipole-allowed transition into the valence state $B^3\Sigma_u^-$. However, the *B* state is complementary [70] to the *E* state and contains a Rydberg admixture which increases with energy (Fig. 1), resulting in a cross section which falls off quickly at higher energies [Fig. 2(a)]. Thus, the assumption of a Gaussian shape is incorrect for the $B \leftarrow X$ transition. The broad Gaussian peaks at 8.68 and 8.93 eV found by Cartwright *et al.* [59], and that at 8.87 eV found by Shyn *et al.* [53] are fitting artifacts necessary to reproduce the asymmetric shape of the $B \leftarrow X$ peak when the analytical model is restricted to symmetric Gaussian line shapes. This interpretation is consistent with the ''curious resemblance'' found by Shyn *et al.* [53] between the differential cross sections for excitation of the *B* and unknown states, at 8.34 and 8.87 eV, respectively. Our coupled-channel results also predict that the broader features in the EEL spectra of the mixed $^3\Sigma_u^-$ states of O_2 in the 7–9.8-eV energy-loss region shift to lower energies and change shape as the impact energy decreases or the scattering angle increases [102], making it even more difficult to perform a simple spectral decomposition.

Similar comments apply to the weaker $^3\Pi_u$ excitations. The coupled-channel analysis shows an even stronger Rydberg-valence interaction than that for the $^3\Sigma_u^-$ states, but the smaller optical transition moment for the valence excitation [28] results in the $^3\Pi_u \leftarrow X^3\Sigma_g^-$ spectrum in the Schumann-Runge region being dominated by a relatively narrow (~ 0.15 eV FWHM), but highly asymmetric peak in the EEL spectrum [Fig. 2(b)] at 9.15 eV, primarily of Rydberg character. This region of the spectrum was modeled by Cartwright *et al.* [59] with a number of narrow Gaussians, but was not mentioned by Shyn *et al.* [53]. At present, it is an open question as to whether any relative change in the small generalized transition moment for the $^3\Pi_u \leftarrow X^3\Sigma_g^-$ valence excitation with varying kinematical conditions will produce a detectable contribution to the EEL spectrum. It is certain, however, that the assignment of the 8.93-eV artifact to this transition by Cartwright *et al.* [59] is incorrect [34].

In summary, we conclude that it is not possible meaningfully to use conventional deconvolution techniques to unravel the contributions of different electronic states to the experimental EEL spectrum when those states are of strongly mixed character. In particular, it is difficult to devise a suitable technique to decompose the Schumann-Runge continuum region of the EEL spectrum of O_2. While a considerable improvement over the Gaussian model could be made by representing the shape of the strong $B \leftarrow X$ continuum by the coupled-channel shape of the optical spectrum, this procedure would still fail to take account of the small shape and position changes which occur when the scattering conditions are changed.

V. SUMMARY AND CONCLUSIONS

The concept of the generalized transition moment has been extended beyond the region of applicability of the first Born approximation and used in the analysis of new electron energy-loss spectra for O_2, which have been measured at intermediate impact energies. A coupled-channel theoretical treatment of the strongly mixed Rydberg and valence states, transitions to which dominate the optically allowed spectrum, has been used to explain the relative intensities of many unusual features occurring in the 7–11.2-eV energy-loss region. For these electronically excited states of $^3\Sigma_u^-$ and $^3\Pi_u$ symmetry, the evolution of the shape of the corresponding electron energy-loss spectrum as the scattering conditions are changed is controlled essentially by one parameter: the ratio of the diabatic generalized transition moments into the Rydberg and valence components of the mixed electronic states. The observed behavior of relative intensities in the EEL spectra of O_2 indicates that the Rydberg GETM decreases away from the optical value much faster than the valence GETM as the momentum transferred in the collision increases, in a similar way for both the $^3\Sigma_u^- \leftarrow X\,^3\Sigma_g^-$ and $^3\Pi_u \leftarrow X\,^3\Sigma_g^-$ transitions.

The results of the coupled-channel analysis indicate that the shapes of the more diffuse spectral features are generally asymmetric and that such features may shift slightly as the scattering conditions are changed. This implies that the simplistic Gaussian–line-shape-based models, which have been employed previously in attempts to decompose the diffuse part of the electron energy-loss spectrum for O_2 into contributions from different electronic states, are unlikely to have given meaningful results. As a consequence of the Rydberg-valence interactions, it has also been found that some vibrational levels of the mixed states give rise to features in the electron energy-loss spectrum which are anomalously strong at the low impact energies and large scattering angles for which optically allowed transitions are expected to decline in relative intensity. These persistent lines are easily confused with those from the optically forbidden transitions which increase in relative intensity under such conditions, and the coupled-channel-GETM technique is thus a valuable aid to the assignment of features in electron energy-loss spectra.

ACKNOWLEDGMENTS

The authors are grateful to Professor M. A. Morrison and Professor C. E. Brion for informative discussions on aspects of electron-molecule scattering, and thank Professor A. R. P. Rau and Professor E. Weigold for critically reading the manuscript. We would also like to thank Dr. M. A. Dillon and Professor C. E. Brion for providing data files of their experimental measurements, Professor R. J. Buenker for communicating unpublished diabatic *ab initio* generalized electronic transition moments, and Dr. T. A. York for supplying a copy of his Ph.D. thesis.

[1] D. C. Cartwright, W. J. Hunt, W. Williams, S. Trajmar, and W. A. Goddard III, Phys. Rev. A **8**, 2436 (1973).

[2] T. A. York and J. Comer, J. Phys. B **16**, 3627 (1983).

[3] J. C. Nickel, P. W. Zetner, G. Shen, and S. Trajmar, J. Phys. E **22**, 730 (1989), and references therein.

[4] M. Allan, J. Phys. B **28**, 4329 (1995).

[5] M. J. Brunger and P. J. O. Teubner, Phys. Rev. A **41**, 1413 (1990), and references therein.

[6] A. G. Middleton, M. J. Brunger, P. J. O. Teubner, M. W. B. Anderson, C. J. Noble, G. Woeste, K. Blum, and C. Fullerton, J. Phys. B **27**, 4057 (1994).

[7] M. A. Dillon, in *Creation and Detection of the Excited State*, edited by A. A. Lamola (Marcel Dekker, New York, 1971), pp. 375–428.

[8] A. Skerbele and E. N. Lassettre, J. Chem. Phys. **44**, 4066 (1966).

[9] J. P. Doering, J. Chem. Phys. **71**, 20 (1979).

[10] E. N. Lassettre, A. Skerbele, M. A. Dillon, and K. J. Ross, J. Chem. Phys. **48**, 5066 (1968).

[11] W. Harshbarger, W. R. Skerbele, and E. N. Lassettre, J. Chem. Phys. **54**, 3784 (1971).

[12] E. N. Lassettre, Can. J. Chem. **47**, 1733 (1969), and references therein.

[13] E. N. Lassettre and A. Skerbele, J. Chem. Phys. **54**, 1597 (1971).

[14] K. L. Klump and E. N. Lassettre, J. Chem. Phys. **60**, 4830 (1974).

[15] The $E\,^3\Sigma_u^-$ state of O_2 is labeled as the B' state by some authors. We prefer the nomenclature suggested by K. P. Huber and G. Herzberg, *Molecular Spectra and Molecular Structure*, *IV Constants of Diatomic Molecules* (Van Nostrand Reinhold, New York, 1979), p. 494.

[16] J. Geiger and B. Schröder, J. Chem. Phys. **49**, 740 (1968).

[17] M. Dillon, M. Kimura, R. J. Buenker, G. Hirsch, Y. Li, and L. Chantranupong, J. Chem. Phys. **102**, 1561 (1995).

[18] R. J. Buenker and S. D. Peyerimhoff, Chem. Phys. Lett. **34**, 225 (1975).

[19] R. J. Buenker and S. D. Peyerimhoff, Chem. Phys. **8**, 324 (1975).

[20] R. J. Buenker and S. D. Peyerimhoff, Chem. Phys. Lett. **36**, 415 (1975).

[21] R. J. Buenker, S. D. Peyerimhoff, and M. Peric, Chem. Phys. Lett. **42**, 383 (1976).

[22] Y. Tanaka, J. Chem. Phys. **20**, 1728 (1952).

[23] R. D. Hudson, Rev. Geophys. Space Phys. **9**, 305 (1972).

[24] W. F. Chan, G. Cooper, and C. E. Brion, Chem. Phys. **170**, 99 (1993).

[25] B. R. Lewis, S. T. Gibson, M. Emami, and J. H. Carver, J. Quant. Spectrosc. Radiat. Transfer **40**, 1 (1988).

[26] M. Yoshimine, J. Chem. Phys. **64**, 2254 (1976).

[27] D. H. Katayama, S. Ogawa, M. Ogawa, and Y. Tanaka, J. Chem. Phys. **67**, 2132 (1977).

[28] P. S. Julienne, D. Neumann, and M. Krauss, J. Chem. Phys. **64**, 2990 (1976).

[29] L. C. Lee, T. G. Slanger, G. Black, and R. L. Sharpless, J. Chem. Phys. **67**, 5602 (1977).

[30] S. T. Gibson and B. R. Lewis, J. Electron Spectrosc. Relat. Phenom. **80**, 9 (1996).

[31] J. B. Nee and P. C. Lee, J. Phys. Chem. A **101**, 6653 (1997).

[32] P. C. Lee and J. B. Nee, J. Chem. Phys. **112**, 1763 (2000).

[33] S. L. Guberman and A. Dalgarno, J. Geophys. Res. **84**, 4437 (1979).

[34] A. C. Allison, S. L. Guberman, and A. Dalgarno, J. Geophys. Res. **87**, 923 (1982).

[35] J. P. England, B. R. Lewis, S. T. Gibson, and M. L. Ginter, J. Chem. Phys. **104**, 2765 (1996).

[36] The nomenclature J for the lowest adiabatic state of $^3\Pi_u$ symmetry is introduced in Sec. IV B.

[37] E. F. van Dishoeck, M. C. van Hemert, A. C. Allison, and A. Dalgarno, J. Chem. Phys. **81**, 5709 (1984).

[38] F. H. Mies, Mol. Phys. **41**, 953 (1980).

[39] F. H. Mies, Mol. Phys. **41**, 973 (1980).

[40] L. Torop, D. G. McCoy, A. J. Blake, J. Wang, and T. Scholz, J. Quant. Spectrosc. Radiat. Transfer **38**, 9 (1987).

[41] J. Wang, D. G. McCoy, A. J. Blake, and L. Torop, J. Quant. Spectrosc. Radiat. Transfer **38**, 19 (1987).

[42] J. Wang, A. J. Blake, D. G. McCoy, and L. Torop, J. Quant. Spectrosc. Radiat. Transfer **40**, 501 (1988).

[43] E. N. Lassettre, S. M. Silverman, and M. E. Krasnow, J. Chem. Phys. **40**, 1261 (1964).

[44] S. M. Silverman and E. N. Lassettre, J. Chem. Phys. **40**, 2922 (1964).

[45] R. H. Huebner, R. J. Celotta, S. R. Mielczarek, and C. E. Kuyatt, J. Chem. Phys. **63**, 241 (1975).

[46] C. E. Brion, K. H. Tan, M. J. van der Wiel, and Ph. E. van der Leeuw, J. Electron Spectrosc. Relat. Phenom. **17**, 101 (1979).

[47] S. Trajmar, W. Williams, and A. Kuppermann, J. Chem. Phys. **56**, 3759 (1972).

[48] S. Trajmar, D. C. Cartwright, and R. I. Hall, J. Chem. Phys. **65**, 5275 (1976).

[49] S. Trajmar, D. C. Cartwright, and W. Williams, Phys. Rev. A **4**, 1482 (1971).

[50] S. Trajmar, D. F. Register, and A. Chutjian, Phys. Rep. **97**, 219 (1983).

[51] S. Trajmar and D. C. Cartwright, in *Electron Molecule Interactions and Their Applications*, edited by L. G. Christophorou (Academic, New York, 1984), Vol. 1, pp. 154–250.

[52] Y. Itikawa, A. Ichimura, K. Onda, K. Sakimoto, K. Takayanagi, Y. Hatano, M. Hayashi, H. Nishimura, and S. Tsurubuchi, J. Phys. Chem. Ref. Data **18**, 23 (1989).

[53] T. W. Shyn, C. J. Sweeney, A. Grafe, and W. E. Sharp, Phys. Rev. A **50**, 4794 (1994).

[54] T. W. Shyn, C. J. Sweeney, and A. Grafe, Phys. Rev. A **49**, 3680 (1994).

[55] K. Wakiya, J. Phys. B **11**, 3913 (1978).

[56] H. A. Bethe, Ann. Phys. (Leipzig) **5**, 325 (1930).

[57] E. N. Lassettre, A. Skerbele, and M. A. Dillon, J. Chem. Phys. **50**, 1829 (1969).

[58] M. Shugard and A. U. Hazi, Phys. Rev. A **12**, 1895 (1975).

[59] D. C. Cartwright, N. A. Fiamengo, W. Williams, and S. Trajmar, J. Phys. B **9**, L419 (1976).

[60] M. Allan, J. Phys. B **25**, 1559 (1992).

[61] M. Allan, Chem. Phys. Lett. **225**, 156 (1994).

[62] However, traditional units of eV and Å are used for energy and internuclear distance, respectively, in the presentation of parameters and results.

[63] N. F. Lane, Rev. Mod. Phys. **52**, 29 (1980).

[64] In fact, according to B. I. Schneider, Phys. Rev. A **14**, 1923 (1976), the Born-Oppenheimer approximation may also be applicable in cases of resonant scattering where the adiabatic-nuclei approximation fails.

[65] E. S. Chang and U. Fano, Phys. Rev. A **6**, 173 (1972).

[66] M. A. Morrison, Aust. J. Phys. **36**, 239 (1983).

[67] Consistent with the assumption of a short collision time, the incident electron spends little time near the nuclei and does not contribute to the electronic potential-energy curves governing the nuclear motion.

[68] This suggestion follows from consideration of a fixed-nuclei scattering amplitude with slow explicit dependences on R and v', within the framework of the R-centroid approximation [R. W. Nicholls, J. Quant. Spectrosc. Radiat. Transfer **2**, 433 (1962)].

[69] C. E. Brion and A. Hamnett, Adv. Chem. Phys. **45**, 1 (1981).

[70] H. Lefebvre-Brion and R. W. Field, *Perturbations in the Spectra of Diatomic Molecules* (Academic, Orlando, 1986), pp. 29–40, 209–212, 344–349.

[71] A. C. Allison, A. Dalgarno, and N. W. Pasachoff, Planet. Space Sci. **19**, 1463 (1971).

[72] B. R. Lewis, L. Berzins, and J. H. Carver, J. Quant. Spectrosc. Radiat. Transf. **36**, 209 (1986).

[73] B. R. Lewis, S. S. Banerjee, and S. T. Gibson, J. Chem. Phys. **102**, 6631 (1995).

[74] Throughout this work, we use the *hat* to distinguish the pure diabatic electronic state (e.g., $\hat{B}$) from the corresponding adiabatic electronic state (e.g., B), with the convention that the diabatic and adiabatic states become indistinguishable at large R values where the coupling is taken to approach zero.

[75] B. R. Lewis, S. T. Gibson, M. Emami, and J. H. Carver, J. Quant. Spectrosc. Radiat. Transfer **40**, 469 (1988).

[76] B. R. Lewis and J. P. England (unpublished).

[77] J. P. England, B. R. Lewis, and M. L. Ginter, J. Chem. Phys. **105**, 1754 (1996).

[78] Y. Li, M. Honigmann, K. Bhanuprakash, G. Hirsch, R. J. Buenker, M. A. Dillon, and M. Kimura, J. Chem. Phys. **96**, 8314 (1992).

[79] B. R. Johnson, J. Chem. Phys. **69**, 4678 (1978).

[80] P. C. Cosby (private communication).

[81] In fact, the $5p\pi_u$ Rydberg state is also involved in the formation of the E' potential-energy curve, but the current model, which includes only the $3p\pi_u$ and $4p\pi_u$ Rydberg states, should be adequate to describe the $E'(0)$ level.

[82] K. Dressler, Ann. Isr. Phys. Soc. **6**, 141 (1983).

[83] The adiabaticity parameter $\zeta = V_{\hat{B}\hat{E}}/\Delta G_E$, where $V_{\hat{B}\hat{E}}$ is the electrostatic interaction matrix element between the diabatic electronic states, and ΔG_E is the separation of the first vibrational levels of the upper adiabatic state formed by the avoided crossing. This parameter provides a measure of the applicability of the adiabatic or diabatic pictures to the mixed states. Near adiabatic behavior occurs for $\zeta \gg 1$, near-diabatic behavior for $\zeta \ll 1$, while for $\zeta \approx 1$, the amount of basis-state mixing in either representation is large.

[84] The energy scale for the CC calculations is expected to be reliable since the calculations were based on very-high-resolution optical spectra of known accuracy.

[85] The uncertainty in the CC oscillator strengths is expected to be $\sim 5\%$, comprising contributions from uncertainties in the very-high-resolution optical oscillator strengths on which the CC model is based, together with uncertainties in the fitting procedure. Furthermore, an extrapolation uncertainty can be expected in the Bethe-Born factor used by Chan *et al.* [24] to normalize their experimental oscillator strengths, which was based on a calibration point at 26-eV energy loss.

[86] Except for the broader features, the intensities are height-width products determined by fitting Fano profiles to the computed rotationless resonances. Intensities of the broader features ($B \leftarrow X$, $J \leftarrow X$) are effective height-width products determined as $0.637\times$ the directly integrated rotationless cross sections. As a result, the optical-limit intensity ratios plotted in Fig. 4 *differ*, in general, from the corresponding ratios of the integrated intensities, but the r dependence of the ratios is insensitive to the definition of the intensities.

[87] H. Park, P. J. Miller, W. A. Chupka, and S. D. Colson, J. Chem. Phys. **89**, 6676 (1988).

[88] Transitions into mixed $^1\Pi_u$ and $^1\Delta_u$ levels [J. P. England, B. R. Lewis, and M. L. Ginter, J. Chem. Phys. **103**, 1727 (1995)] may also contribute to the intensity of the 10.80-eV EEL peak. However, the dominant $3d,4s \leftarrow X$ vibrational structure observed in the $E_r = 2$ eV, $\theta = 90°$ spectrum militates against any significant contribution from this source.

[89] Since the optically forbidden contributions dominate in the $E_r = 2$ eV, $\theta = 90°$ spectrum, corresponding to the highest momentum-transfer values plotted in Fig. 6, the scaling factors employed were determined by matching the relative intensities of the peaks for only this spectrum, after the application of small computed corrections for the effects of the optically allowed transitions.

[90] Initial experimental intensity ratios were determined using the width-height products of peaks in the EEL spectra. These were converted into ratios suitable for comparison with the computed values of Fig. 4 using correction factors determined by the analysis of instrumentally-degraded theoretical spectra.

[91] B. R. Lewis (unpublished).

[92] Corrections for the contributions of $F \leftarrow X$ transitions were performed exactly for $K^2 = 0$ using experimental optical oscillator strengths, and approximately for nonzero K^2 using computed relative intensities. These corrections generally became much less significant at higher K^2 because of rapid fall off in the relative $F \leftarrow X$ intensities.

[93] Since the $J \leftarrow X$ feature at 9.15 eV exists only as an inflection in the experimental cross section, the width of this feature was assumed to be independent of the scattering conditions, and equal to the theoretical value, in estimating the integrated intensities.

[94] The methods of this work do not allow us to compute the relative intensities of the $^3\Pi_u \leftarrow X\,^3\Sigma_g^-$ and $^3\Sigma_u^- \leftarrow X\,^3\Sigma_g^-$ systems in the EEL spectra without reference to experiment. Therefore, the calculated $F \leftarrow X(0,0)$ to $E \leftarrow X(0,0)$ intensity ratios in Fig. 8 were obtained from the computed constituent spectra of Fig. 5(a), each of which has been optimized by comparison with the experimental spectra of Fig. 5(b).

[95] The only np Rydberg states of O_2 that are as yet unobserved are the $np\pi_\omega\,^1\Sigma_u^-$ states. Energies for these states that have been predicted recently [B. R. Lewis, S. T. Gibson, S. S. Banerjee, and H. Lefebvre-Brion, J. Chem. Phys. **113**, 2214

(2000)] are well separated from the $F(0)$ energy.
[96] P. C. Hill, Ph.D. thesis, The Australian National University, 1991.
[97] R. J. Buenker and Y. Li (private communication).
[98] The *ab initio* values [97] plotted in Fig. 9 apply at an internuclear distance $R=2.3$ a.u.
[99] The lowest impact-energy spectrum discussed here has $E_r=2$ eV, i.e., about an order of magnitude greater than the vibrational spacing. We assume that the AN approximation remains valid under this condition.
[100] Non-Franck-Condon effects appear to be evident in the $3s\sigma_g\,{}^3\Pi_g$ vibrational intensities in the $E_r=2$ eV, $\theta=90°$ spectrum in Fig. 5(b), presumably due to the effects of negative-ion resonances.
[101] M. Ogawa, K. R. Yamawaki, A. Hashizume, and Y. Tanaka, J. Mol. Spectrosc. **55**, 425 (1975).
[102] Although not immediately apparent from Fig. 5(b), these small shifts are also observed experimentally. In order to obtain quantitative agreement between the experimental shifts and those computed using the CC method, it is necessary to allow the relative R dependence of the valence ${}^3\Sigma_u^- \leftarrow X\,{}^3\Sigma_g^-$ GETM to vary from the optical value.